






Vibration Response Analysis of an Aircraft Structure in terms of Crashworthiness by using Differential Transformation Method

Aysun SOYSAL^{1,*} , Ibrahim OZKOL² , Erol UZAL³ 

¹ Istanbul Technical University, Department of Mathematical Engineering, 34469, Istanbul, Türkiye

² Istanbul Technical University, Department of Aeronautical Engineering, 34469, Istanbul, Türkiye

³ Istanbul University-Cerhpaşa, Department of Mechanical Engineering, 34320, Istanbul, Türkiye

Highlights

- This paper focuses on vibration analysis of an aircraft structure in terms of crashworthiness.
- A mathematical model of an aircraft structure subjected to a crush loading is derived and solved.
- Effects of a crush load on the vibration characteristics of an aircraft structure are investigated.

Article Info

Received: 30 Oct 2023

Accepted: 26 Apr 2024

Keywords

Crush loading
Vibration analysis
Energy principle
Differential transform
method

Abstract

Due to importance of certification procedure and safety of occupants, crashworthiness is one of the most principal elements to be considered in the design and production of civil and military aircrafts. In the component level, the crashworthiness of an aircraft structure is significantly affected by many factors including the cross-section of the aircraft structure, boundary conditions of the aircraft structure, and applied crush loading to the aircraft structure. The aim of this study is to contribute to the literature on improving the design of aircraft structures in order to increase the energy absorption properties of the aircraft structures and therefore support the crashworthiness capability of the structures by performing vibration analysis. In this context, after deriving the governing equations of an aircraft structure exposed to an axial crush loading, three different applications are conducted to investigate the effects of the axial crush loading on the dynamic characteristics of the aircraft structure. The findings of the study concluded that vibration characteristics of an aircraft structure subjected to an axial crush loading are affected by the boundary conditions of the structure, material of the structure, cross-section of the structure, magnitude of the axial load applied to the structure, and direction of the axial load applied to the structure. In addition, the findings showed that the response of the structure under ultimate axial crush loading varies depending on the geometry of the structure, material of the structure and the direction of the ultimate axial crush loading applied to the structure.

1. INTRODUCTION

Global airlines consume more than 3.5 million tones of oil per day, causing carbon dioxide (CO_2) emitted from aircraft engines to reach alarming levels [1]. Moreover, CO_2 emanating from commercial and military aircraft is expected to reach more than twice as much as the current levels by 2050 [2]. As a precaution against this situation, some modern aircraft configurations, for instance aircrafts flying-V shape, are projected to achieve more than 20% fuel savings when compared to conventional configurations. However, these newly implemented design-type aircraft configurations present some challenges with the design, including the crashworthiness of wing-fuselage structures that have an oval-shaped cross-section leading to a significant reduction in the area under the cabin floor [3]. The design of aircraft structures for crashworthiness (i.e., crashworthiness design) needs ensuring the structural integrity of the structures [4], reducing crash cost for the structures repair [5], and providing the safety of passengers [6], which is the most important one, in the event of a collision. Thus, the crashworthiness design is considered as important as the durability and fatigue [7] of aircraft structures.

Considering the certification standards established by aviation regulatory agencies, modern aircraft manufacturers have used a variety of protection systems regarding the crashworthiness of aircraft structures [8]. The primary goal for protecting the fuselage and structures is the performance [9] and hence crashworthiness of the aircraft structures. On the other hand, at the component level, various energy absorbers have been proposed to evaluate the crashworthiness response of the aircraft structures [10]. Due to their excellent energy absorption characteristic, thin-walled structures (e.g., beams, columns or frames) have been widely used in the fields of the crashworthiness analysis of aircraft structures [11]. Especially thin-walled beams, which have a superior feature in terms of light weight and utilized as reinforcement components in the body of vehicles, have been mostly exploited to investigate the deflection behavior and mechanical properties of the aircraft structures under static and dynamic crush loadings [12]. Moreover, given that evaluating the feasibility of design of an aircraft in the preliminary stage is indispensable importance to preventing cost overruns and minimizing the need for significant design changes [13], the development of low-fidelity models, for instance beam-type structures, to assess the crashworthiness at the preliminary stage of design of aircraft structures is both an attractive and feasible option because these models provide not only low computational cost but also the ability to conduct parametric studies on structure exposed to the crush [3]. On the other hand, according to a study conducted in collaboration with the European Program for the Design of Commercial Aircraft for Crash Survival (CRASURV) [14], numerical analysis studies showed that promising results were achieved by gradually crushing the beams in terms of their energy absorption ability, but experimental tests showed that the design of the beams needed improvement. This situation reveals the necessity of using thin-walled beams in crashworthiness analyzes of aircraft structures to both benefit from their energy absorption ability and obtain the advantages of using simpler models in the preliminary design phase of the structure, while it also reveals that the design of thin-walled beams should be improved.

In the literature, researchers have conducted numerous studies on the design of thin-walled structures to improve and optimize the crashworthiness ability of aircraft structures. Regarding the effects of the design on the energy absorption capacity, Mou et al. [10] researched the damage and energy absorption mechanisms for the lightweight and crashworthiness design of hybrid open-section thin-walled columns. They conducted an experimental study to characterize the mechanical responses and failure morphologies of the structure, and then validated the experimental study with a numerical simulation model. The results of the study showed that open-section thin-walled columns provide a new structural configuration to meet the crashworthiness properties and lightness needs of aircrafts, which are vital in aviation and space-related applications. Liang et al. [15] studied on variable thickness of hybrid multi-cell tube (i.e., based on beam configuration) to investigate the energy absorption characteristics of hybrid structure for the crashworthiness design of the structure facing complex loading conditions. They used a numerical finite element model for different tube configurations. The analysis showed superiority of multi-material hybrid structure over mono-material component. Xue et al. [16] studied the efficiency of the struts and then compared the energy absorption abilities of two different shapes (i.e., strut—C shape and wide-flange shape) to investigate the crashworthiness of an aircraft fuselage and struts under the cabin floor. These studies [10, 15- 16] proved that improving the design of thin-walled structures increases the energy absorption capacity of the structures. However, there are a wide variety of parameters that affect the design of the structures. In terms of cross-sectional area of the structures, Ren and Xiang [17- 19] examined the crashworthiness of aircraft structures with various strut configurations, which were based on aluminum thin walled beams with varied cross sections, by using the finite element approach. Patil and Pangavhane [20] introduced a new square cross-section thin-walled column to increase the crashworthiness of an aircraft structure under axial loading by performing a numerical study via ABAQUS software and then validated the results with an experimental and analytical test. The study indicated that variable thickness square thin-walled column provides better performance than uniform thickness square thin-walled column. Tang et al. [12] examined the bending behaviors of several simple-section thin-walled beams exposed to lateral impact using analytical and numerical methods. In order to determine the effects of geometric shapes of the thin-walled beams on the crashworthiness of the structure, the bending performance was evaluated depending on some design parameters, such as length ratio of rectangular section, height, etc. The study concluded that the beam cross-sectional area affected the bending resistance performance of the thin-walled beams under lateral impact in different ranges. In terms of static load response of the structures, Moas et al. [21] proposed an analytical model including a semicircular graphite epoxy specimen, which models a generic

aircraft frame exposed to a quasi-static load, to investigate the load response and damage behavior of the aircraft frame. In the analysis, the mathematical model of a semicircular frame subjected to a concentrated force was solved, and then they applied the finite element solution to confirm the results of the model. Woodson et al. [22] presented an optimum design of a composite body frame subjected to a static crush loading to improve the crashworthy response of the frame. The fuselage frame was considered as a thin-walled, I-section, and graphite-epoxy frame; and then the analysis was carried out by using a genetic algorithm. In terms of the type of the joining (i.e., boundary condition) of the structure, Collins and Johnson [23] developed a numerical model, called a beam finite element, based on finite element methodology to evaluate the dynamic and static response of thin-walled and open section frames that are common in fuselage construction. In this context, they determined the dynamic characteristics of I shape frames, semicircular frames, and channel section frames. The authors showed that the cross-section and boundary condition of the structure affect the crashworthiness response of the structure. Perez et al. [24] developed a numerical model to optimize open section curved composite frames subjected to a static crush loading to improve energy absorption. They examined a semicircle and I shape frames in the design of flanges; and then the results were obtained for clamped and hinged boundary conditions of the frames by using a generic algorithm. Garofano et al. [9] investigated dynamic response of a regional fuselage barrel section to obtain an optimized skin configuration in a vertical drop test for the crashworthiness characteristics of the structure by using finite element method. In the construction of an aircraft fuselage, struts, joints, and supports were used to connect the cross beams in the cabin floor to the frames and cargo area. The struts connecting the cabin floor to the reinforcement supports were modeled as beam-section elements. The study showed that minor damage was noted to the cabin floor beams via newly introduced configuration design of the skin. In terms of damage behavior of the structure, Zhang et al. [25] conducted an application to investigate the crashworthiness response of an aircraft wing structure under distributed pressure load by using LS-DYNA and ANSYS CFX numerical programs. In the finite element model of the aircraft wing structure, the spars in a box structure were modelled as I-beam. Numerical results showed that during the distributed pressure load, the leading edge of the wing was damaged approximately 70 cm, but the front spar broke the birch into two parts.

The aforementioned literature shows that aircraft structures absorb a huge portion of the kinetic energy of a crush due to their ductile behavior before fracture. Thus, in terms of crashworthiness and the related survivability of the aircraft structures, the design of the aircraft structures need to be improved to avoid or resist severe environments including a crush loading. The aim of this study is to contribute to the literature in order to improve the design of aircraft structures in a way that will increase the energy absorption characteristics of the structures and therefore support the crashworthiness ability of the structures by performing vibration analysis. In this context, a coupled-bending torsion thin-walled beam is taken into account. Considering the aforementioned literature, the present study investigates the crashworthiness performance of the structure (i.e., thin-walled beam) depending on: (i) the change of the boundary conditions of the structure, (ii) the change of an applied static load (including ultimate crush loadings) and directions of the static load, and (iii) the change of the geometric shape of the structure. Moreover, due to the importance of the relationship between the structural parameters and crashworthiness ability of the structure [26], the effects of some structural parameters of the structure on the crashworthiness ability of the structure are investigated. Thus, since many factors affecting the design of the structure are evaluated together in terms of the crashworthiness performance of the structure and, accordingly, the damage behavior, the present study are expected to contribute to the literature due to its wide scope. In the analysis, Differential Transform Method (DTM) is used for the solution of the design problem considered in the present study. DTM is a technique for solving a wide variety of differential equations both analytically and numerically [27- 29]. Furthermore, given that crash experiments are extremely difficult and expensive to perform, the application of DTM to such a design problem is another contribution to the literature because DTM is suitable both for solving uncomplicated design problems manually and calculating them analytically, and for solving complicated design problems numerically through parallel programming with powerful computers. A flow chart that summarizes the stages of the present study is given in Figure 1.

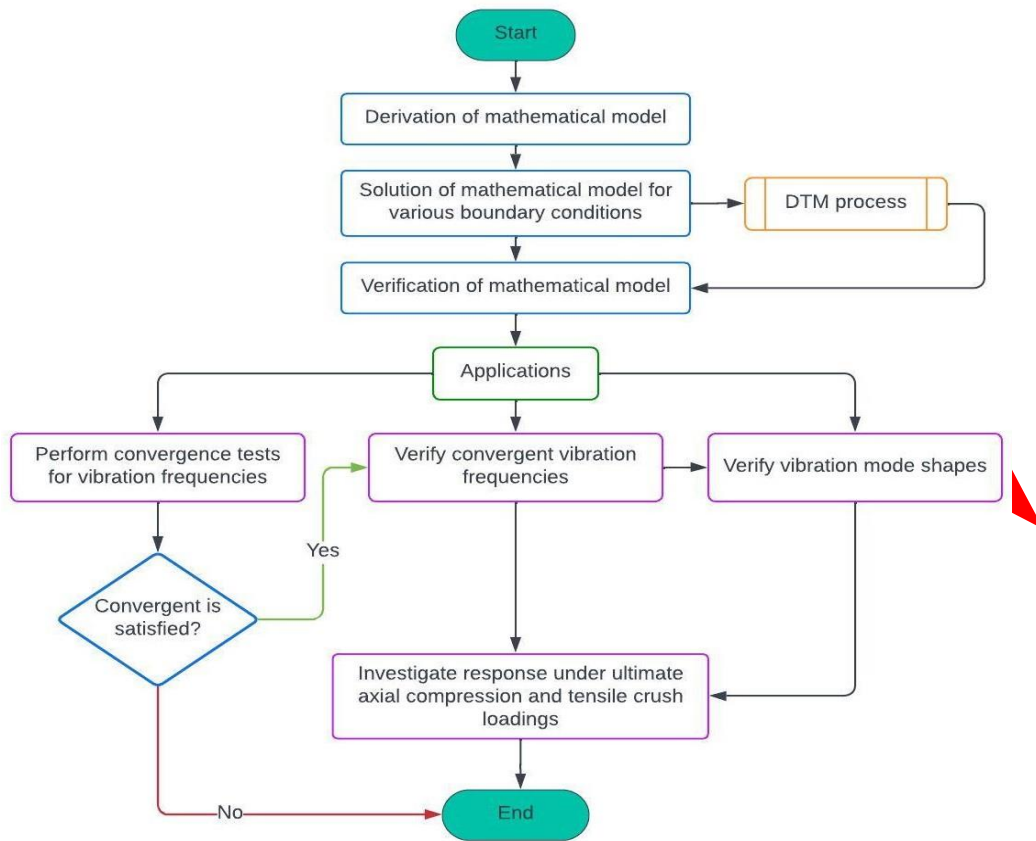


Figure 1. A flowchart that represented the steps of the study

2. MATERIAL AND METHODS

2.1. Derivation of the Mathematical Model

Many engineering structures can be modeled as a flexible beam supporting various intermediate elements [30]. For this reason, beam structures are widely used in vibration analysis studies of aircraft structures and in examining the resistance deviations of the structure against static and dynamic loads [31 - 32]. More specifically, an axially loaded coupled bending torsion beam can be taken into account as an aircraft structure which is subjected to a crush loading because some complete plane and space frames can be represented with reasonable accuracy as ensembles of interconnected axially loaded coupled bending-torsion beams [33]. Moreover, since aluminum alloys have been the main material of structural parts of aircrafts for approximately 90 years due to their known performance, well-established design techniques, manufacturing and reliable inspection methods [34], it is estimated that the active use of aluminum in aircraft structures will continue in today's technological developments. Thus, in the establishment of a mathematical model of an aircraft structure that is exposed to an axial crush loading, a uniform axially loaded coupled bending-torsion thin-walled beam made of an aluminum alloy is considered. A coupled bending-torsion thin-walled beam having airfoil cross section with length L is shown in Figure 2. In Figure 2 (a), $u(x, t)$ is bending translation and $\psi(x, t)$ is torsional rotation of the beam. Further, an axial load P , that represents an axial crush loading, is assumed to act along the center of gravity (i.e., center of mass) of the cross-section of the beam. When P is an axial compressive load, the sign is considered positive (i.e., direction of load inward), as shown in Figure 2 (a). On the other hand, when P is an axial tensile load, the sign is considered negative (i.e., direction of load outward). Additionally, in Figure 2 (a), the mass axis and elastic axis of the beam present respectively the loci of the centroid and shear center of the beam. In Figure 2 (b), $f(x, t)$ and $g(x, t)$ are respectively the distributed external forces and torques, where x denotes distance from the origin and t denotes time.

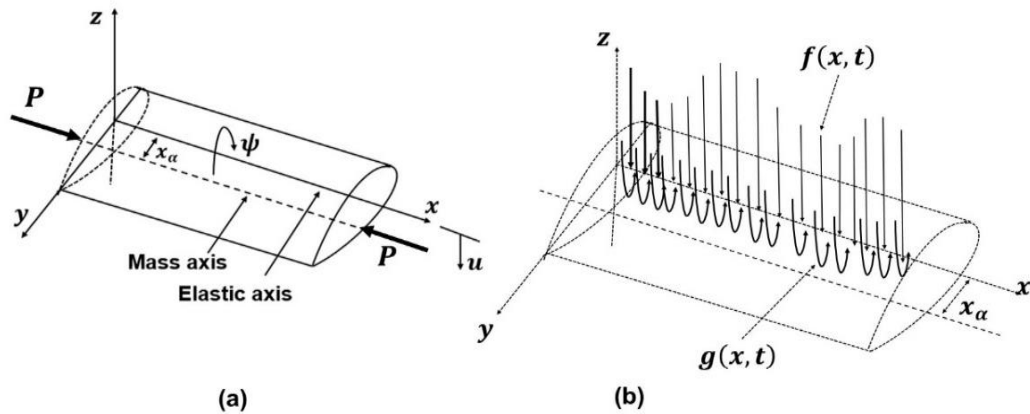


Figure 2. (a) a uniform axially loaded coupled bending-torsion beam on the coordinate system, (b) the distributed external forces and torques applied to the beam

The mathematical model of the motion with damped coefficients of the uniform axially loaded coupled bending-torsion thin-walled beam, representing an aircraft structure exposed to an axial crush loading, can be derived by using energy principle, called the extended Hamilton principle, as follows.

The total potential energy U_{PE} , kinetic energy T_{KE} , and virtual work W_E of the axially loaded coupled bending torsion beam are respectively stated as:

$$U_{PE} = \frac{1}{2} \int_0^L \{EI(u'')^2 - P[(u')^2 + (I_\alpha/m)(\psi')^2] + GJ(\psi')^2\} dx \quad (1)$$

$$T_{KE} = \frac{1}{2} \int_0^L \{m(\dot{u})^2 - 2mx_\alpha \dot{u}\dot{\psi} + I_\alpha(\dot{\psi})^2\} dx, \quad (2)$$

$$W_E = \int_0^L \{f(x, t)u + g(x, t)\psi - c_1 \dot{u}u - c_2 \dot{\psi}\psi\} dx, \quad (3)$$

where EI, GJ, m, x_α , and I_α are respectively bending rigidity, torsional rigidity, mass of the beam per unit length, bending-torsion (i.e., geometric) coupling term, and mass moment of inertia per unit length of the beam. The coefficients c_1 and c_2 are respectively the linear viscous damping terms of per unit length of the beam in bending deformation and torsional deformation. (') and (̇) denote differentiations with respect to space x and time t , respectively.

According to the extended Hamilton's principle, when $L_{KP} = T_{KE} - U_{PE} + W_E$, here L_{KP} is kinetic potential, then $\int_{t_1}^{t_2} dt$ that is evaluated for any arbitrary intervals of time (e.g. t_1, t_2) is stable for a dynamic trajectory. Thus,

$$\delta \int_{t_1}^{t_2} (T_{KE} - U_{PE} + W_E) dt = 0 . \quad (4)$$

Substituting Equations (1)-(3) into Equation (4) and then performing the related integral operations yields the governing differential equations and boundary conditions of the axially loaded uniform coupled-bending torsion thin-walled beam as follows:

(a) The governing differential equations

$$EIu'''' + P(u'' - x_\alpha \psi'') + c_1(\dot{u} - x_\alpha \dot{\psi}) + m(\ddot{u} - x_\alpha \ddot{\psi}) = f(x, t) \quad (5)$$

$$GJ\psi'' - P(\{I_\alpha/m\}\psi'' - x_\alpha u'') - c_2\dot{\psi} + c_1x_\alpha\dot{u} + mx_\alpha\ddot{u} - I_\alpha\ddot{\psi} = g(x, t) \quad (6)$$

with

$$\theta = u' \quad (\text{Bending rotation}) \quad (7)$$

$$M = -EIu'' \quad (\text{Bending moment}) \quad (8)$$

$$S = EIu''' + P(u' - x_\alpha\psi') \quad (\text{Shear force}) \quad (9)$$

$$T = GJ\psi' - \{PI_\alpha/m\}\psi' + Px_\alpha u' \quad (\text{Torque}) \quad (10)$$

(b) The boundary conditions (BCs) for different end conditions are:

$$\text{Clamped-Free (C-F): } u = \theta = \psi = 0, \quad S = M = T = 0 \quad (x = 0, L) \quad (11)$$

$$\text{Clamped-Clamped (C-C): } u = \theta = \psi = 0, \quad u = \theta = \psi = 0 \quad (x = 0, L) \quad (12)$$

$$\text{Simply Supported-Simply Supported (S-S): } u = \psi = M = 0, \quad u = \psi = M = 0 \quad (x = 0, L) \quad (13)$$

2.2. Solution of the Model

For free vibration analysis with undamped case, the dynamic characteristics of a uniform axially loaded coupled bending-torsion thin-walled beam can be found by equalizing the external force $f(x, t)$, external torque $g(x, t)$, and damping coefficients c_1 and c_2 to zero. Then, the solutions of the equations given in Equations (5) – (6) are assumed to be of the form

$$u(x, t) = U_n(x)\cos(\omega_n t + \phi_n) \quad (14)$$

$$\psi(x, t) = \Psi_n(x)\cos(\omega_n t + \phi_n) \quad (15)$$

where $U_n(x)$ and $\Psi_n(x)$ are vibration modes, ω_n is the vibration frequency, ϕ_n is phase angles, and $n = 1, 2, 3, \dots$

Substituting Equations (14) – (15) into Equations (5) – (6) and Equations (11) – (13) reduces the partial differential equations with associated boundary conditions to ordinary differential equations with associated boundary conditions as follows:

$$EIU_n'''' + P(U_n'' - x_\alpha\Psi_n'') - m\omega_n^2(U_n - x_\alpha\Psi_n) = 0 \quad (16)$$

$$GJ\Psi_n'' + \{P/m\}(mx_\alpha U_n'' - I_\alpha\Psi_n'') - \omega_n^2(mx_\alpha U_n - I_\alpha\Psi_n) = 0 \quad (17)$$

with the boundary conditions given in Equations (11) – (13) when $u = U_n$ and $\psi = \Psi_n$.

Then, DTM is applied to solve Equations (16) – (17) with the related boundary conditions. According to the theory of DTM [35], an analytical function $f(x)$ is expanded to a power series with the center x_0 in domain of $f(x)$. For this purpose, the differential transform and inverse transform of $f(x)$ are respectively stated by $F_D[k]$ and $f_D[x]$ as follows:

$$F_D[k] = \frac{1}{k!} \left(\frac{d^k f(x)}{dx^k} \right) \Big|_{x=x_0} \quad (18)$$

$$f_D[x] = \sum_{k=0}^{\infty} (x - x_0)^k F_D[k]. \quad (19)$$

There are some differential transformation rules regarding the application of DTM. These rules vary depending on type of the function in differential equations and boundary conditions. The differential transformation rules of DTM for various functions and operations are given in reference [36]. Taking these rules into account, each function in the differential equations and boundary conditions is represented in a

new form. Thus, by applying the related differential transformation rules given in [36] to both the ordinary differential equations given in Equations (16) – (17) and boundary conditions given in Equations (11) – (13), a set of algebraic equations is obtained as follows:

$$U_D[k + 4] = \frac{a(k + 1)(k + 2)U_D[k + 2] + b(k + 1)(k + 2)\Psi_D[k + 2] + cU_D[k] + d\Psi_D[k]}{(k + 1)(k + 2)(k + 3)(k + 4)} \quad (20)$$

$$\Psi_D[k + 2] = \frac{e(k + 1)(k + 2)U_D[k + 2] + f(k + 1)(k + 2)\Psi_D[k + 2] + gU_D[k] + h\Psi_D[k]}{(k + 1)(k + 2)} \quad (21)$$

with

$$\Theta_D[k] = \sum_{k=0}^N kU_D[k]L^{k-1} \quad (22)$$

$$M_D[k] = \sum_{k=0}^N k(k - 1)U_D[k]L^{k-2} \quad (23)$$

$$S_D[k] = \sum_{k=0}^N k(k - 1)(k - 2)U_D[k]L^{k-3} - a \sum_{k=0}^N kU_D[k]L^{k-1} - b \sum_{k=0}^N k\Psi_D[k]L^{k-1} \quad (24)$$

$$T_D[k] = \sum_{k=0}^N k\Psi_D[k]L^{k-1} - f \sum_{k=0}^N k\Psi_D[k]L^{k-1} - e \sum_{k=0}^N kU_D[k]L^{k-1} \quad (25)$$

where

$$a = -\frac{P}{EI}, \quad b = \frac{Px_\alpha}{EI}, \quad c = \frac{m\omega_n^2}{EI}, \quad d = -\frac{mx_\alpha\omega_n^2}{EI}, \quad (26)$$

$$e = -\frac{Px_\alpha}{GJ}, \quad f = \frac{PI_\alpha}{mGJ}, \quad g = \frac{mx_\alpha\omega_n^2}{GJ}, \quad h = -\frac{\omega_n^2 I_\alpha}{GJ} \quad (27)$$

and $U_D[k]$ and $\Psi_D[k]$ are differential transform of $U_n(x)$ and $\Psi_n(x)$, respectively; $\Theta_D[k]$, $M_D[k]$, $S_D[k]$, and $T_D[k]$ are the differential transform of the natural boundary conditions given in Equations (7) – (10). Moreover, in Equations (22) – (25), N denotes the number of terms included in the application of DTM; and the value of N is determined depending on the convergence of the vibration frequencies. Thereafter, based on the vibration frequencies, the vibration mode shapes of the beam are obtained by using the inverse transform formulation given in Equation (19) as follows:

$$U_n(x) = \sum_{k=0}^N U_D[k]x^k \quad (28)$$

$$\Psi_n(x) = \sum_{k=0}^N \Psi_D[k]x^k. \quad (29)$$

The pseudocode related with application of DTM to solve the Equations (20) – (21) with the boundary conditions given in Equations (22) – (25) is presented in Algorithm 1. The Equations (28) – (29) are conjunction with the boundary conditions stated in Equations (11) – (13).

```

Step 1. Read the data  $EI, GJ, m, I_\alpha, x_\alpha, L, P$ .
Step 2. Compute coefficients  $a, b, c, d, e, f, g, h$ .
Step 3. Set  $U_D[i] = \alpha, U_D[i + 1] = \beta, \Psi_D[i] = \gamma, i = 0, 1, 2, 3$ .
    For  $k = 0, \dots, N$ 
        Compute  $U_D[k + 4]$ 
        Compute  $\Psi_D[k + 2]$ 
    End
    For  $k = 0, \dots, N$ 
        Compute BC1
        Compute BC2
        Compute BC3
    End
Step 4. Solve the following system of equations:

$$M_{j1}^{(n)}(\omega)\alpha + M_{j2}^{(n)}(\omega)\beta + M_{j3}^{(n)}(\omega)\gamma = 0, \quad j = 1, 2, 3.$$

Step 5. Check the convergence of the solution of the system given in Step 4.

$$|\omega_j^{(n)} - \omega_j^{(n-1)}| \leq \varepsilon$$

    where  $\omega_j^{(n)}$ : the  $j$ th estimated vibration frequency corresponding to  $n$ ,
     $\omega_j^{(n-1)}$ : the  $j$ th estimated vibration frequency corresponding to  $n - 1$ .
    If iterative refinement is needed, go back to Step 5.
Step 6. Select the real parts of the vibration frequencies obtained in Step 5 as the resulting vibration frequencies.
Step 7. Compute the vibration mode shapes  $U_n(x)$  and  $\psi_n(x)$  by using inverse transformation functions.
    
```

Algorithm 1. The pseudocode of DTM (ε : is a tolerance value, BC: boundary condition)

3. RESULTS AND DISCUSSION

To verify the derived governing equations and the solution of the equations, three applications, which include three thin-walled beams with different geometries, were considered in this study. The profiles and properties of the beams were given in Figure 3 and Table 1, respectively.

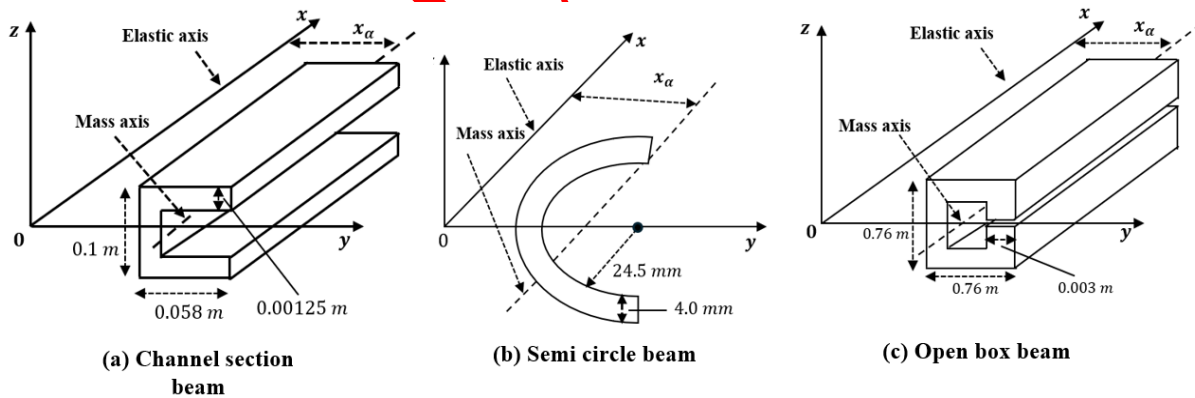


Figure 3. Profiles of three thin-walled beams with different geometries

Table 1. Material properties of three thin-walled beams with different geometries

Thin-walled beams	EI_x (Nm^2)	GJ (Nm^2)	m (kg/m)	I_α ($kg * m$)	$x_\alpha(m)$	$L(m)$
Channel cross-section beam [37, 38]	0.974×10^5	11.21	2.095	0.00725	0.03771	1.28
Semi-circle cross-section beam [38, 39]	6380.14	43.46	0.835	0.000501	0.0155	0.82
Open box cross-section beam (with an axial slit) [40, 41]	5.8×10^4	78.3	2.45	0.02	0.08	5.0

The graphics and tables related with the results of the applications were obtained in Mathematica environment with the codes developed by the user. For each application, the followings were realized for the C-F, C-C, and S-S boundary conditions: (i) Convergence tests were performed for vibration frequencies: The first six convergent vibration frequencies are obtained, and the effect of the axial crush loading on the convergent vibration frequencies are determined, (ii) Convergent vibration frequencies are verified: The convergent vibration frequencies obtained in the first stage are verified with the similar studies borrowed from the available literature. Then, relationships between an axial crush loading P and geometric coupling property of the structure x_α are examined in terms of the vibration frequencies, and (iii) Vibration mode shapes are verified: The vibration mode shapes associated with the convergent vibration frequencies are obtained and then compared with similar studies from existing literature when comparison is possible. Moreover, the effects of an axial crush loading, including ultimate axial compressive and tensile load, on the vibration mode shapes are determined.

3.1. Convergence Tests to Obtain Convergent Vibration Frequencies

In order to obtain the first six convergent vibration frequencies and determine the influence of an axial crush loading on the convergent vibration frequencies depending on the boundary conditions, the convergence tests were performed and then the results of the tests were shown in Figures 4-12. In these figures, the amount of the axial crush loading was taken as $P = 2560\text{ N}$ [38] for the channel cross-section thin-walled beam, $P = 1790\text{ N}$ [38] for the semi-circle cross-section thin-walled beam, and $P = 2500\text{ N}$ for the open box cross-section thin-walled beam. As shown in the figures, it was seen that when the number of terms included in the application of DTM (N) are increased from 10 to 60, the convergence of the vibration frequencies are increased (i.e., as more terms are included in DTM, greater convergence is achieved). Moreover, for each application, compared to the vibration frequencies in the case of absence of the axial crush loading, when the axial crush loading acts in compression ($P < 0$), the vibration frequencies of the aircraft structures decrease, but when it acts in tension ($P > 0$), the vibration frequencies increase. Furthermore, as seen in Figures 4-6, it was observed that to attain the first six convergent vibration frequencies of the aircraft structures for the C-F boundary condition, the channel, semi-circle, and open box cross-section thin-walled beams require respectively the first sixty, thirty, and forty terms in DTM. On the other hand, for the C-C and S-S boundary conditions, as presented in Figures 7-12, the channel, semi-circle, and open box cross-section thin-walled beams require respectively the first fifty, forty, and fifty terms in DTM.

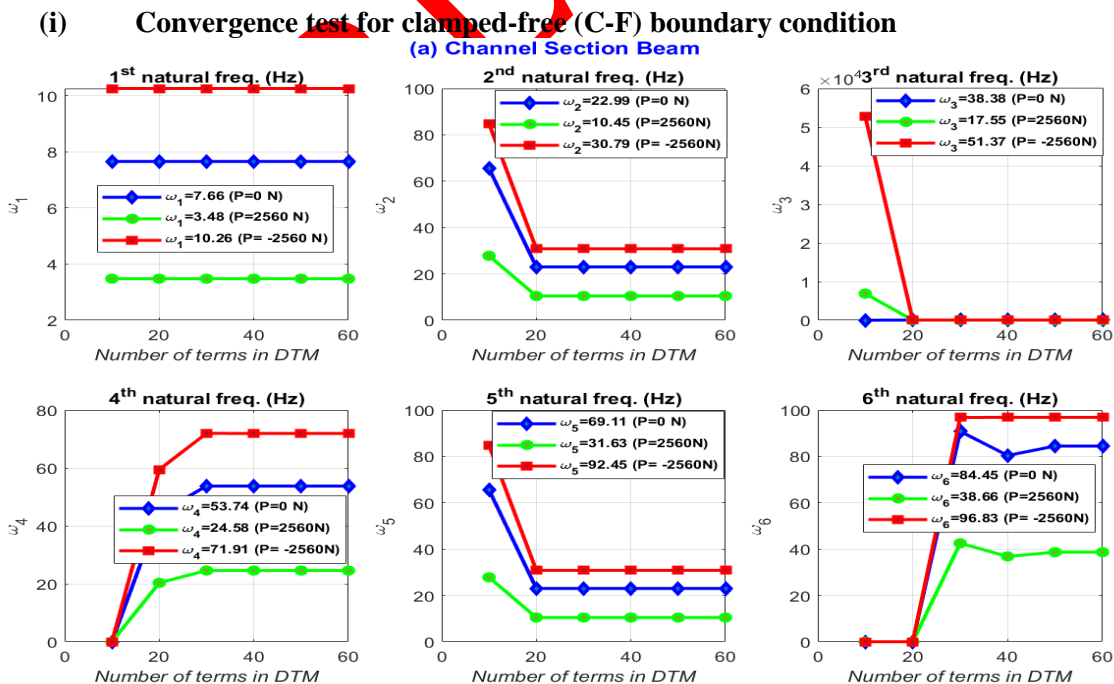


Figure 4. Convergence test for the aircraft structure with channel cross-section for C-F boundary condition

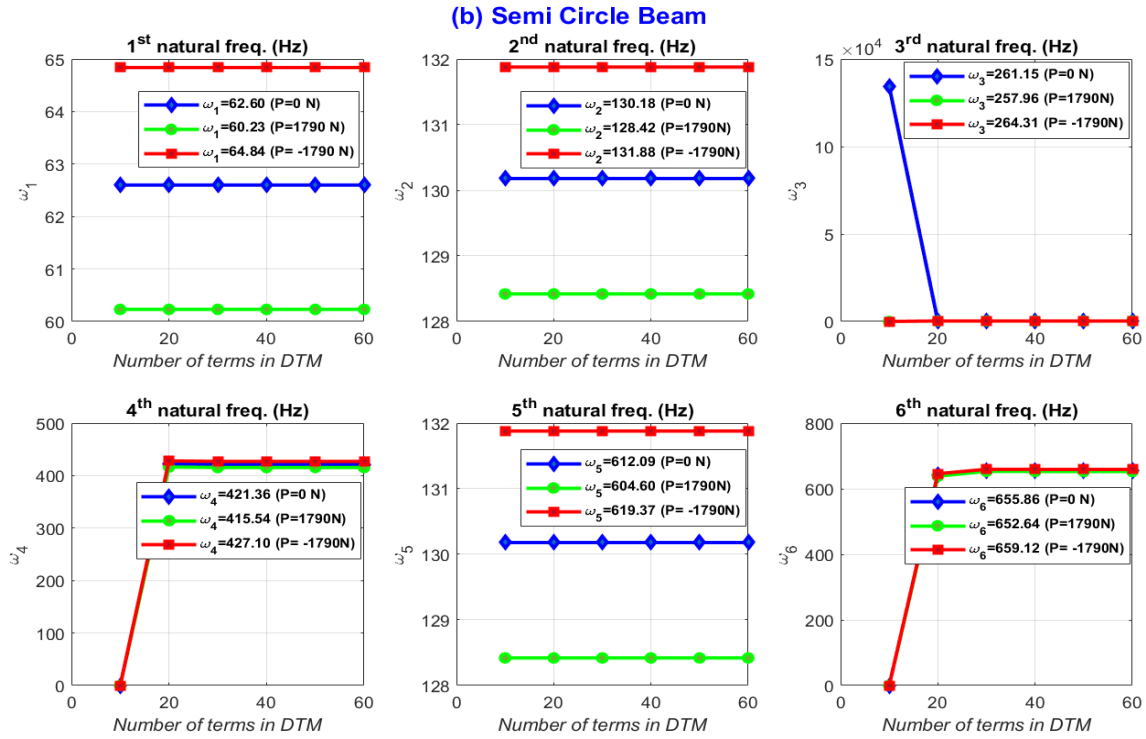


Figure 5. Convergence test for the aircraft structure with semi-circle cross-section for C-F boundary condition

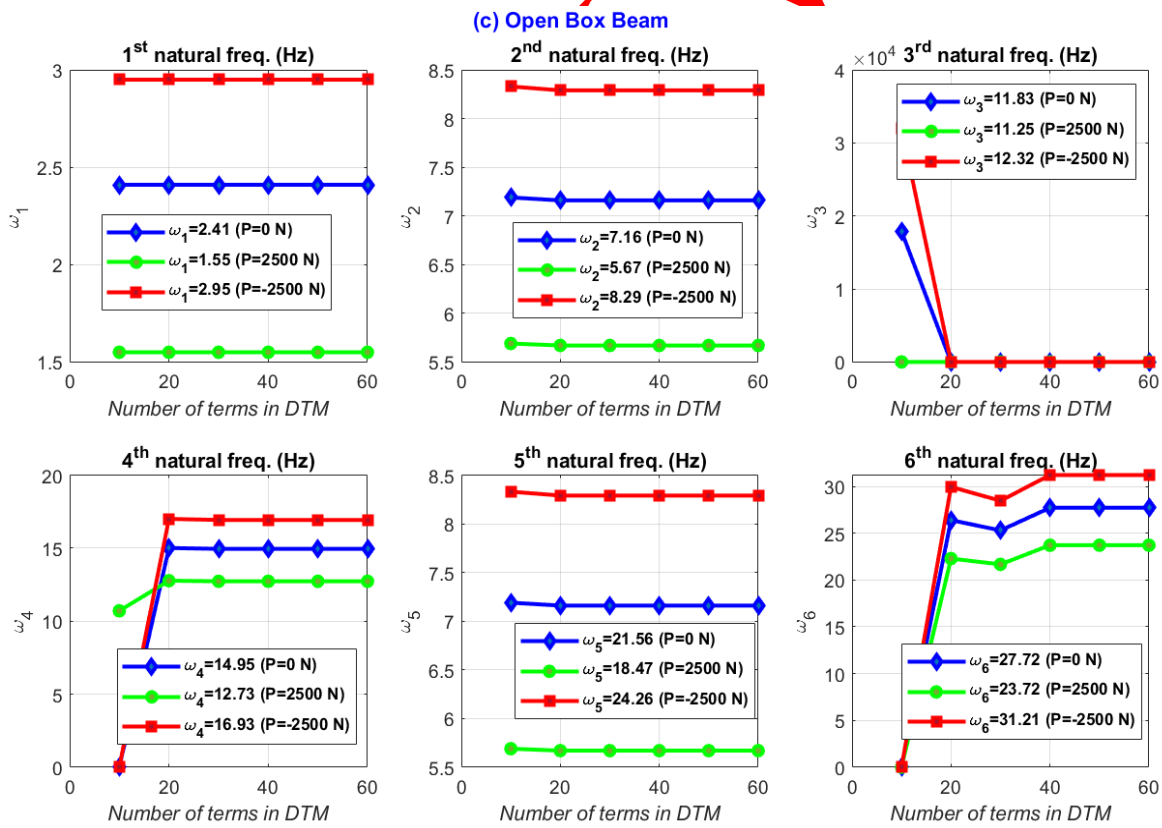


Figure 6. Convergence test for the aircraft structure with open box cross-section for C-F boundary condition

(ii) Convergence test for clamped-clamped (C-C) boundary condition

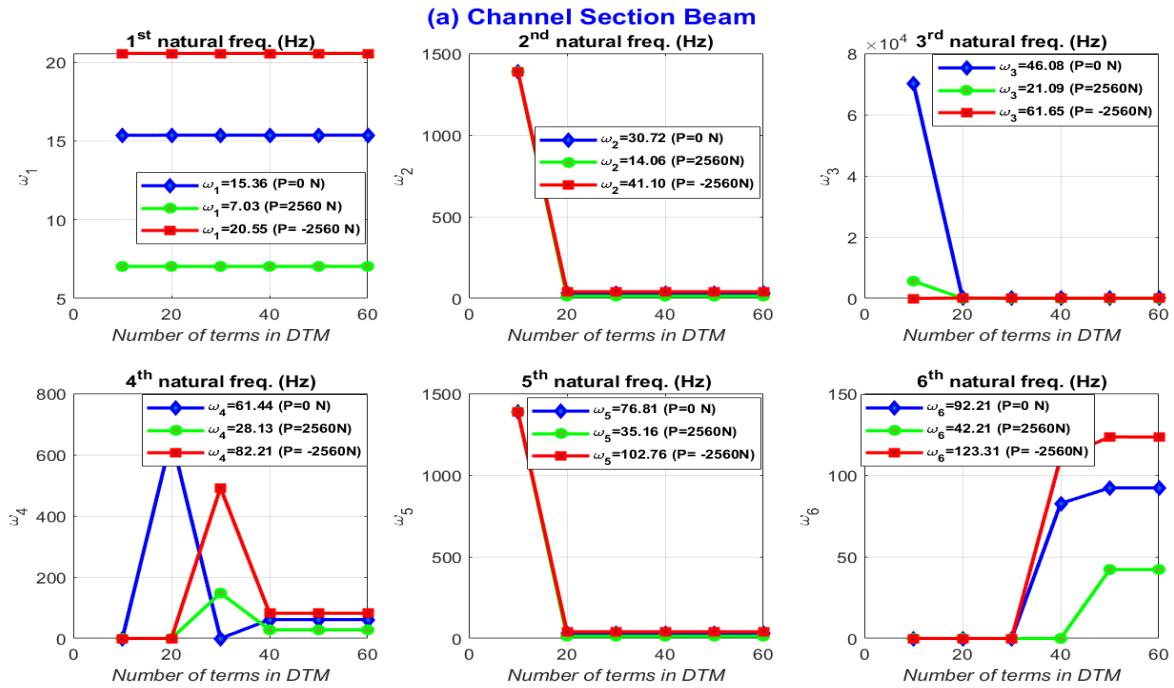


Figure 7. Convergence test for the aircraft structure with channel cross-section for C- C boundary condition

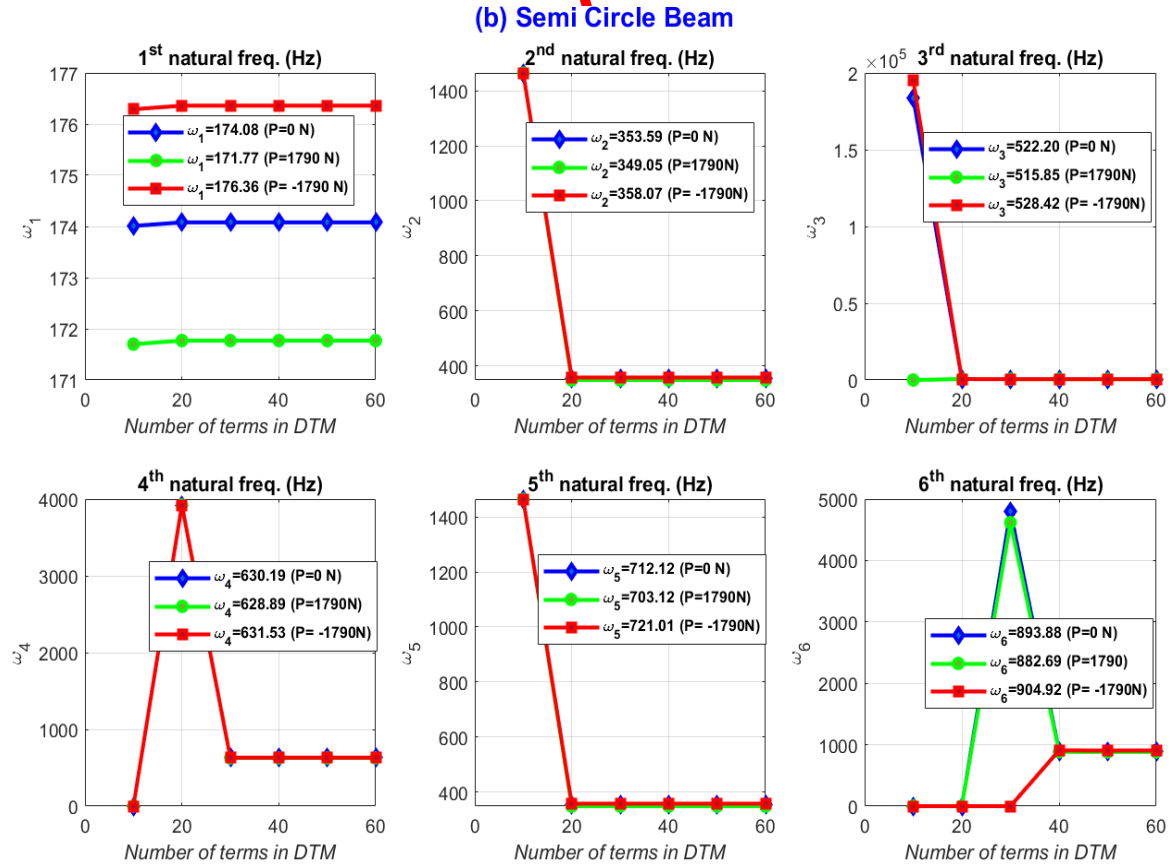


Figure 8. Convergence test for the aircraft structure with semi-circle cross-section for C- C boundary condition

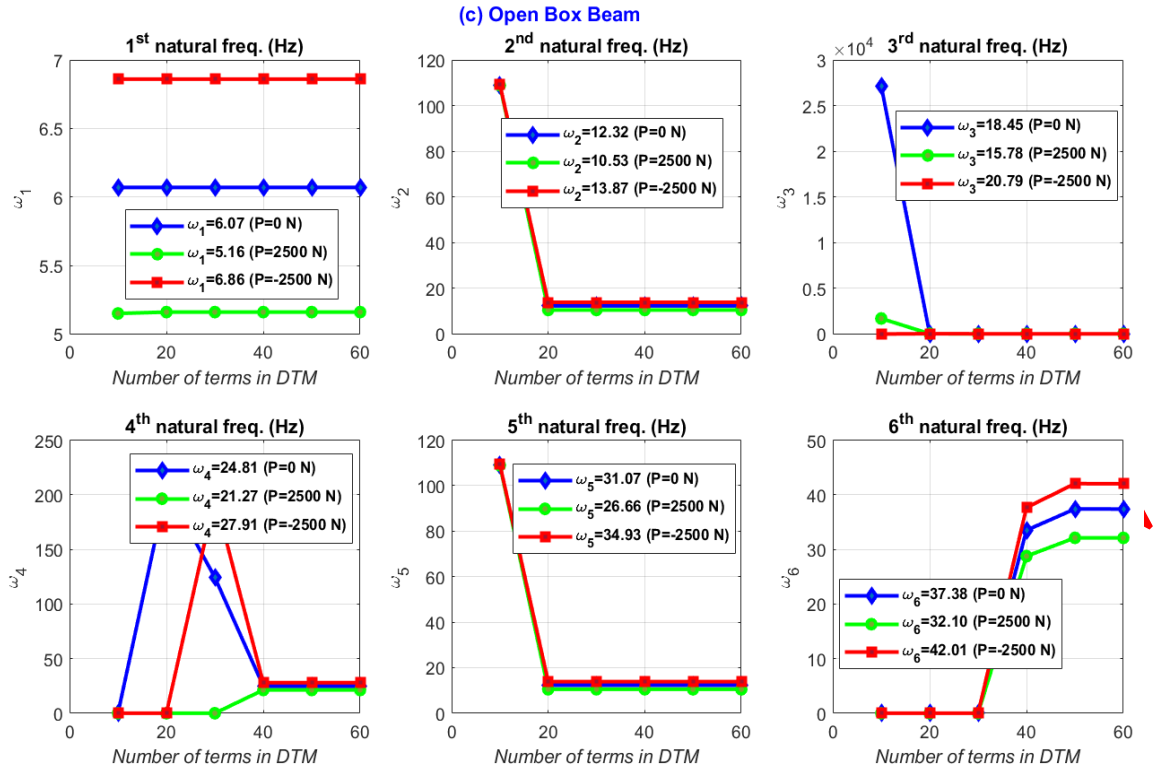


Figure 9. Convergence test for the aircraft structure with open box cross-section for C- C boundary condition

(iii) Convergence test for simply supported-simply supported (S-S) boundary condition

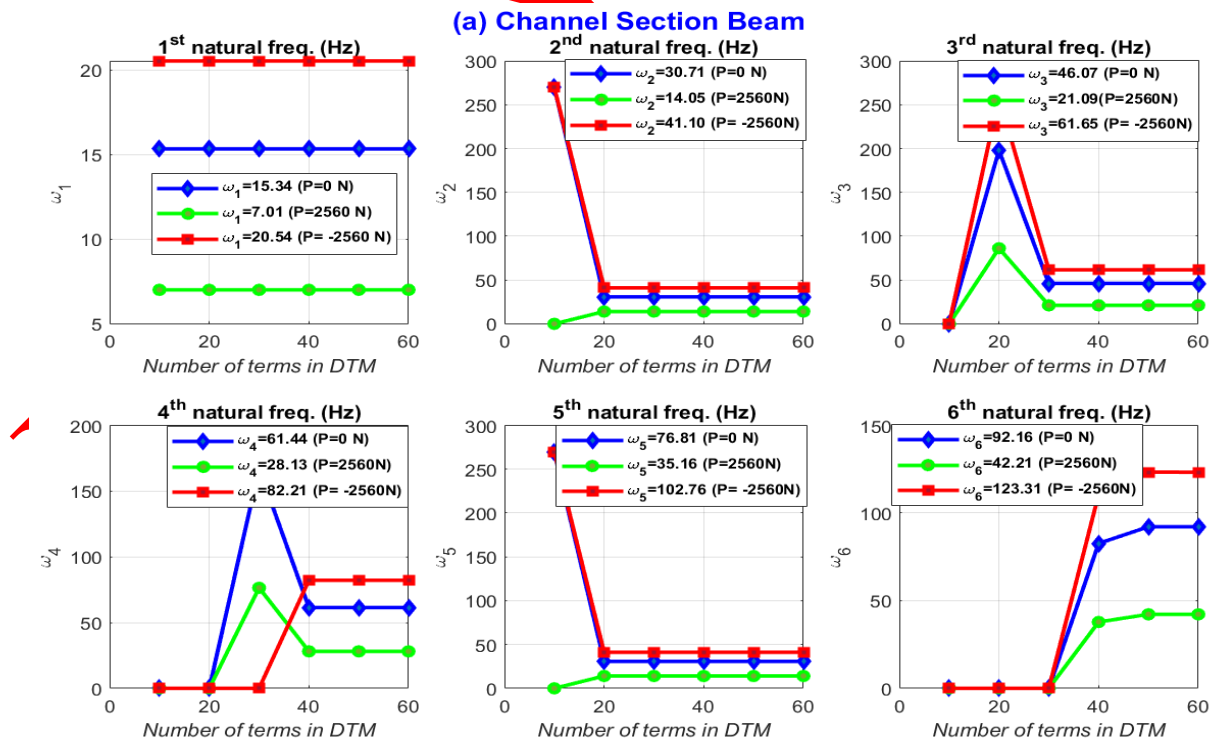


Figure 10. Convergence test for the aircraft structure with channel cross-section for S - S boundary condition

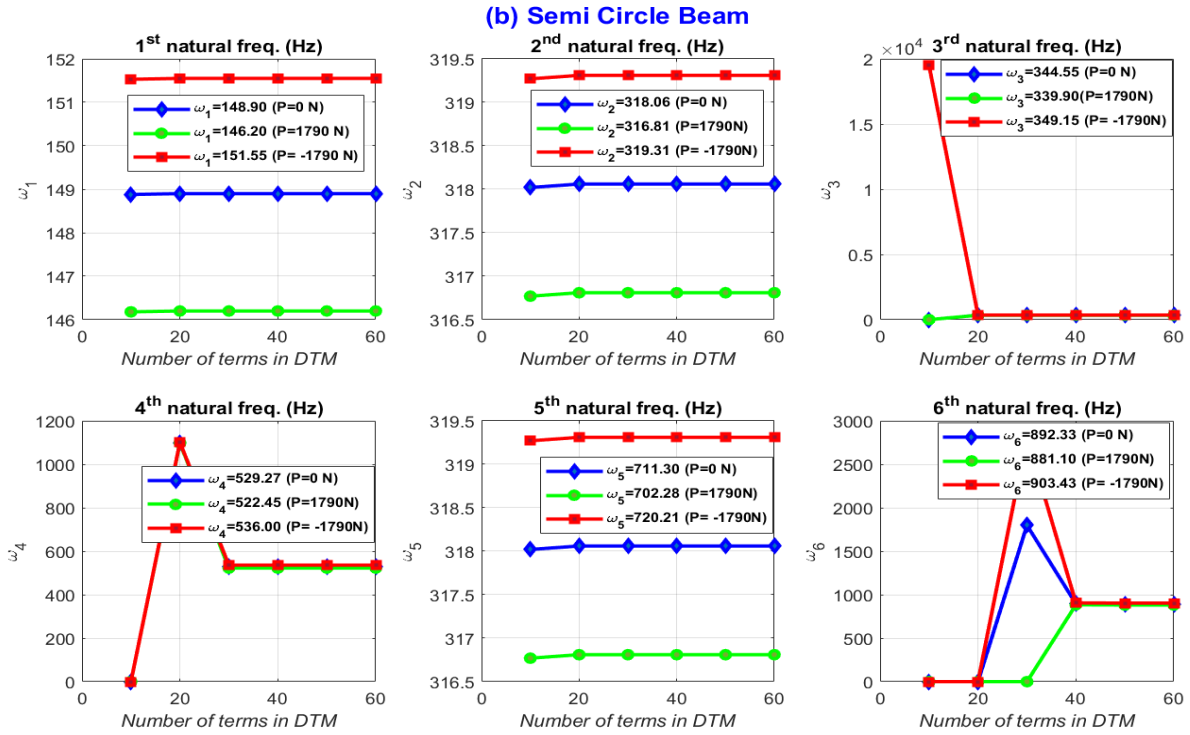


Figure 11. Convergence test for the aircraft structure with semi-circle cross-section for S - S boundary condition

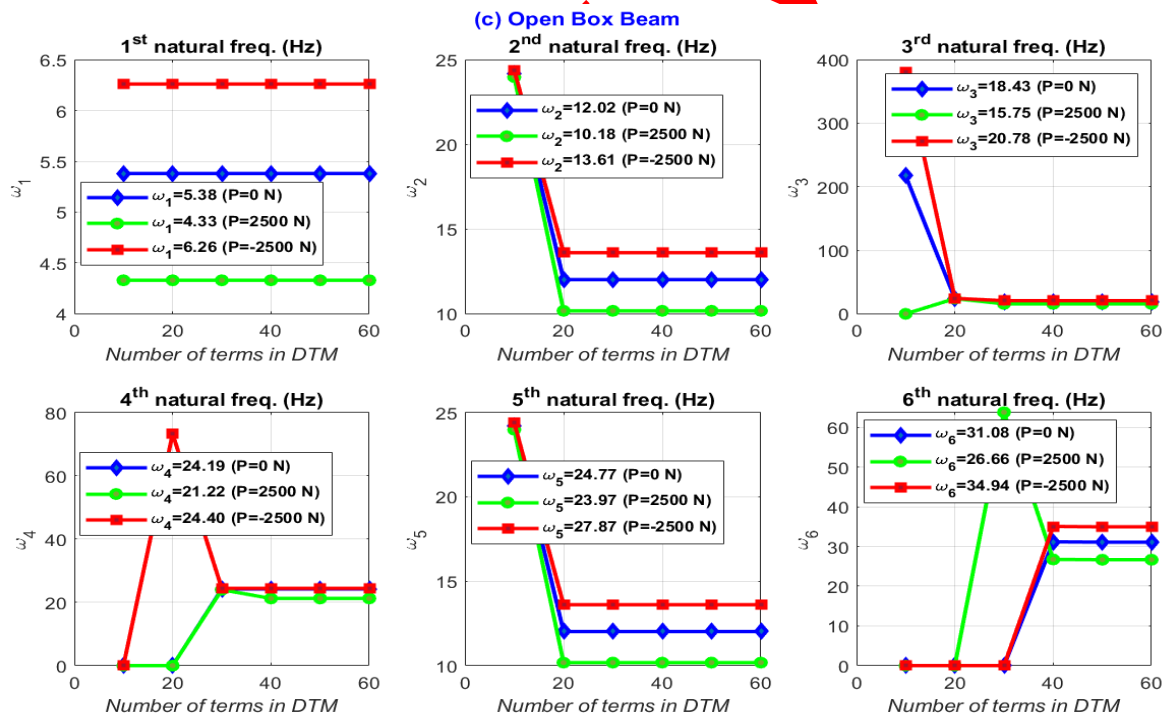


Figure 12. Convergence test for the aircraft structure with open box cross-section for S - S boundary Condition

3.2. Verification of Convergent Vibration Frequencies

To verify the convergent vibration frequencies and then examine the relations between an axial crush loading and geometric coupling property of an aircraft structure depending on the boundary conditions, cross-section of the aircraft structure, and the direction of the axial crush loading, the vibration frequencies of the aircraft structure were obtained by including 100 terms in DTM, and then the results were presented

in Table 2 – Table 4. As indicated in these tables, in the Coupled case (Coupled) (i.e., $x_\alpha \neq 0$), the vibration frequencies of the aircraft structure were found to be good agreement with the results of the studies in reference [37] and reference [38] for the channel cross-section thin-walled beam, in reference [38] for the semi-circle cross-section thin-walled beam, and in reference [39] for the open box cross-section thin-walled beam in terms of relative error ϵ_{rel} for the C-F, C-C, and S-S boundary conditions. Additionally, regarding the relations between an axial crush loading and geometric couplig property of the aircraft structure depending on the boundary condition and direction of the axial crush loading, it was found that (i) regardless of the direction of the axial crush loading, the geometric coupling term has a reduce effect for the C-F boundary condition and almost no effect for the C-C and S-S boundary conditions for the channel cross-section thin-walled beam (when compered the vibration frequencies in Coupled case with the vibration frequencies in Uncoupled (UnC.) (i.e., $x_\alpha = 0$) case) and (ii) irrespective of the direction of the axial crush loading, there is no any specific effect (for instance, increase or reduce effect) of the geometric coupling term on the vibration frequencies of the semi-circle and open box cross-section thin-walled beams for the C-F, C-C, and S-S boundary conditions.

Table 2. Vibration frequencies of the aircraft structure with channel cross-section

		$P = 0 N$						$P = 2560 N$ (Compression)				$P = -2560 N$ (Tension)	
		UnC.	Coupled				UnC.	Coupled			UnC.	Coupled	
B	NF (Hz)	DTM	DTM	Ref. [37]	ϵ_{rel} (%)	Ref. [38]	ϵ_{rel} (%)	DTM	DTM	Ref. [38]	ϵ_{rel} (%)	DTM	DTM
C-F	ω_1	7.68	7.66	7.66	0.00	7.66	0.00	3.51	3.48	3.48	0.00	10.28	10.26
	ω_2	23.04	22.99	22.99	0.00	22.99	0.00	10.55	10.45	10.45	0.00	30.83	30.79
	ω_3	38.40	38.38	38.38	0.00	38.38	0.00	17.58	17.55	17.56	0.06	51.38	51.37
	ω_4	53.76	53.74	-	-	53.74	0.00	24.62	24.58	24.60	0.08	71.93	71.91
	ω_5	69.12	69.11	-	-	69.11	0.00	31.65	31.63	31.65	0.06	74.24	92.45
	ω_6	73.64	84.45	-	-	-	-	38.68	38.66	-	-	92.48	96.83
C-C	ω_1	15.36	15.36	15.36	0.00	15.35	0.07	7.03	7.03	7.03	0	20.55	20.55
	ω_2	30.72	30.72	30.71	0.00	30.72	0.00	14.07	14.06	14.07	0.07	41.10	41.10
	ω_3	46.08	46.08	46.08	0.00	46.08	0.00	21.10	21.09	21.10	0.05	61.65	61.65
	ω_4	61.44	61.44	-	-	61.44	0.00	28.14	28.13	28.15	0.07	82.20	82.20
	ω_5	76.81	76.81	-	-	76.81	0.00	35.17	35.16	35.19	0.09	102.76	102.76
	ω_6	92.16	92.16	-	-	-	-	42.21	42.21	-	-	123.31	123.31
S-S	ω_1	15.36	15.34	15.34	0.00	15.34	0.00	7.03	7.01	7.01	0.00	20.54	20.54
	ω_2	30.72	30.71	30.71	0.00	30.71	0.00	14.07	14.06	14.06	0.00	41.10	41.10
	ω_3	46.07	46.07	46.07	0.00	46.08	0.02	21.10	21.10	21.10	0.00	61.65	61.65
	ω_4	61.44	61.44	-	-	61.44	0.00	28.14	28.13	28.15	0.07	82.21	82.21
	ω_5	76.81	76.81	-	-	76.81	0.00	35.17	35.16	35.19	0.09	102.76	102.76
	ω_6	92.16	92.16	-	-	-	-	42.20	42.21	-	-	123.31	123.31

3.3. Verification of Vibration Mode Shapes

To verify the vibration mode shapes associated with the convergent vibration frequencies (by using the results of existing similar studies in the literature where comparison was possible) and determine the effects of an axial crush loading on the vibration mode shapes of an aircraft structure (i.e., a thin-walled beam) depending on the boundary conditions, cross-section of an aircraft structure, and direction of the axial crush loading, the vibration mode shapes were plotted and given in Figure 13 – Figure 30. It should be noted that, in these figures, the torsional rotation ψ times coupling term x_α was plotted for the torsional displacement, so that at any cross-section along the length of the structure, the displacement of the center of gravity due to the torsional effect alone (ψx_α) can be directly compared to the bending displacement. In this context, for each application: (i) The vibration mode shapes of the aircraft structure with the C-F boundary condition in the absence and presence (including its direction) of the axial crush loading were drawn, and then the results were compared with similar studies in the literature to verify the application of DTM. Then, using the same DTM codes developed, the changes in the vibration mode shapes were investigated for the C-C and S-S boundary conditions in the absence and presence (including its direction) of the axial crush loading

and (ii) According to the safety factor used in the design of aerospace structures, the limit (i.e., ultimate) loads that the structure can carry are determined depending on the cross-sectional area of the structure for the aluminum alloy AL2024 T351 (This material is the most used in aviation and aircraft structures and has very strong strength [34]). Then, under these ultimate loads, the vibration mode shapes of the structure at different boundary conditions are determined with respect to cross-sectional area of the structure and the direction of the axial crush loading.

Table 3. Vibration frequencies of the aircraft structure with semi-circle cross-section

		$P = 0 \text{ N}$				$P = 1790 \text{ N}$ (Compression)				$P = -1790 \text{ N}$ (Tension)	
		UnC.	Coupled		UnC.	Coupled		UnC.	Coupled		
BC	NF (Hz)	DTM	DTM	Ref. [38]	ϵ_{rel} (%)	DTM	DTM	Ref. [38]	ϵ_{rel} (%)	DTM	DTM
C-F	ω_1	72.74	62.60	62.60	0.00	70.10	60.23	60.23	0.00	75.27	64.84
	ω_2	89.79	130.18	130.18	0.00	88.67	128.42	128.42	0.00	90.89	131.88
	ω_3	269.38	261.15	261.15	0.00	266.03	257.96	257.96	0.00	272.69	264.31
	ω_4	448.97	421.36	421.36	0.00	443.39	415.54	415.54	0.00	454.48	427.10
	ω_5	455.89	612.09	612.09	0.00	453.01	604.60	604.60	0.00	458.75	619.37
	ω_6	628.56	655.86	-	-	620.75	652.64	-	-	636.28	659.12
C-C	ω_1	179.59	174.08	174.08	0.00	177.35	171.77	171.77	0.00	181.79	176.36
	ω_2	359.18	353.58	353.58	0.00	354.71	349.05	349.05	0.00	363.59	358.07
	ω_3	462.90	522.20	522.20	0.00	461.83	515.85	515.85	0.00	463.97	528.42
	ω_4	538.77	630.19	630.19	0.00	532.07	628.89	628.89	0.00	545.38	631.53
	ω_5	718.36	712.12	712.12	0.00	709.42	703.12	703.12	0.00	727.18	721.01
	ω_6	897.95	893.88	-	-	886.78	882.69	-	-	908.97	904.92
S-S	ω_1	179.59	148.90	148.90	0.00	177.35	146.20	146.20	0.00	181.79	151.55
	ω_2	204.20	318.06	318.06	0.00	202.24	316.81	316.81	0.00	206.14	319.31
	ω_3	359.18	344.55	344.55	0.00	354.71	339.90	339.90	0.00	363.59	349.15
	ω_4	538.77	529.27	529.27	0.00	532.07	522.45	522.45	0.00	545.38	536.00
	ω_5	718.36	711.30	711.30	0.00	709.42	702.28	702.28	0.00	727.18	720.21
	ω_6	816.81	892.33	-	-	814.86	881.10	-	-	818.76	903.43

Table 4. Vibration frequencies of the aircraft structure with open box cross-section

		$P = 0 \text{ N}$				$P = 2500 \text{ N}$ (Compression)		$P = -2500 \text{ N}$ (Tension)	
		UnC.	Coupled		UnC.	Coupled	UnC.	Coupled	
BC	NF (Hz)	DTM	DTM	Ref. [40]	ϵ_{rel} (%)	DTM	DTM	DTM	DTM
C-F	ω_1	3.12	2.41	2.41	0.00	2.63	1.55	3.51	2.95
	ω_2	3.44	7.16	7.16	0.00	2.69	5.67	4.06	8.29
	ω_3	9.36	11.83	11.83	0.00	8.07	11.25	10.54	12.32
	ω_4	15.64	14.95	14.95	0.00	13.45	12.73	17.56	16.93
	ω_5	21.58	21.56	21.55	0.05	18.83	18.47	22.34	24.26
	ω_6	21.89	27.72	27.72	0.00	20.79	23.72	24.59	31.21
C-C	ω_1	6.26	6.07	6.07	0.00	5.38	5.16	7.03	6.86
	ω_2	12.51	12.32	12.32	0.00	10.76	10.53	14.05	13.87
	ω_3	18.77	18.45	18.45	0.00	16.14	15.78	21.08	20.79
	ω_4	21.96	24.81	24.81	0.00	21.52	21.27	22.20	27.91
	ω_5	25.03	31.07	31.07	0.00	21.62	26.66	28.10	34.93
	ω_6	31.29	37.38	37.38	0.00	26.90	32.10	35.13	42.01
S-S	ω_1	6.26	5.38	6.21	13.37	5.38	4.33	7.03	6.26
	ω_2	9.67	12.02	10.82	11.09	9.12	10.18	10.18	13.61
	ω_3	12.51	18.43	18.27	0.88	10.76	15.75	14.05	20.78
	ω_4	18.77	22.19	22.31	8.43	16.14	21.22	21.08	24.40
	ω_5	25.03	26.77	26.39	6.14	21.52	23.97	28.10	27.87
	ω_6	31.29	31.08	30.95	0.42	26.90	26.66	35.13	34.94

3.1.1. Vibration mode shapes of aircraft structures

(i) Vibration mode shapes depending on cross section, boundary conditions, and an axial crush loading (including its direction)

- (a) The first four vibration mode shapes of the aircraft structure with the channel cross-section for the C-F boundary condition were drawn in the absence and presence of the axial crush loading and then the results were given in Figure 13. When the vibration modes (mode shapes) in the case of the axial compressive load (Figure 13 (e)-(h)) were compared with the vibration modes with the same data in reference [38], a very high agreement was found between the studies. This shows that the DTM codes developed provide quite accurate results in calculating the vibration modes of the channel cross-section aircraft structure under the axial compressive crush loading P (when $P = 2560 N$). Moreover, as seen in Figure 13, it has been observed that, compared to the absence of axial crush loading, whether the axial load is compressive or tensile does not make a difference in the vibration modes for a load of $P = 2560 N$. Furthermore, the vibration modes for the C-C and S-S boundary conditions were obtained in the absence and presence of axial load (taking into account the sign-dependent condition) and then given in Figure 14 and Figure 15, respectively. As can be seen from these figures, as in the C-F boundary condition, there was no any change in the vibration mode shapes (including the sign) in the presence of axial load, compared to the absence of axial load (when $P = 2560 N$). In addition, the relative measurements of the displacement between bending motion and torsional motion indicated that in the generated vibration modes, the torsional motion is particularly prominent in the first five modes for the C-F, C-C, and S-S boundary conditions.
- (b) For the C-F boundary condition, the first four vibration mode shapes of the aircraft structure with the semi-circle cross-section were plotted in the absence and presence of the axial crush loading, and then the results were presented in Figure 19. Compared the vibration mode shapes in Figure 19 (e)-(h) with the vibration modes with the same data in reference [38], it was found that there is a very good agreement between the studies, which proves that the DTM codes developed are quite reliable. Moreover, for the C-C and S-S boundary conditions, the first four vibration mode shapes of the structure with the semi-circle cross-section were presented in the absence and presence (including its direction) of the axial crash loading in Figure 20 – Figure 21, respectively. As can be seen from these figures, it was observed that, compared to the absence of axial load, whether the axial crush loading is compressive or tensile does not create a difference in the vibration modes for an axial load of $P = 1790 N$. Additionally, regarding the relative measurements of the displacement between bending motion and torsional motion, the generated vibration modes showed that all vibration modes are in coupled mode in the first four modes for the C-F, C-C, and S-S boundary conditions.
- (c) The first four vibration mode shapes of the aircraft structure with the open box cross-section were obtained in the absence and presence of the axial crush loading (including its direction) for the C-F, C-C, and S-S boundary conditions, and then the results were presented in Figure 25 – Figure 27. Compared the vibration mode shapes in Figure 25 (a)-(d) with the vibration modes with the same data in reference [40], it was observed that there is a very good agreement between the studies. This agreement proves the verification of the DTM codes developed. Moreover, regarding the effect of the axial crush loading P (when $P = 2500 N$) on the vibration mode shapes for the C-F, C-C, and S-S boundary conditions, while the axial crush loading had a negligible effect on the vibration modes in terms of amplitudes, it made a relatively significant change in terms of the form of the resulting vibration mode shapes, as shown in Figure 25 – Figure 27. Furthermore, the direction of the axial crush loading was also effective in this change. In addition, regarding the relative measurements of the displacement between bending motion and torsional motion for the C-F, C-C, and S-S boundary conditions, the all vibration modes generated were found to be in the coupled mode for the first five modes.

(ii) **Vibration mode shapes under ultimate axial compression load P_{yield} and ultimate axial tensile load $P_{tensile}$ depending on boundary conditions**

- (a) In general engineering practice, the structures are designed for a factor of security (FOS) times the ultimate load [42]. The FOS is at least 1.5 in aerospace structures [42]. On the other hand, using the data in reference [37], the cross-sectional area A of the aircraft structure with the channel cross-section was found to be $2.6688e - 04 m^2$. According to mechanical properties of aerospace aluminium alloy AL 2024-T351 given in [34], the yielding strength σ_{yield} and ultimate tensile strength $\sigma_{tensile}$ are $324 MPa$ and $428 MPa$, respectively. Thus the ultimate axial compression load P_{yield} (i.e., $\left(\frac{\sigma_{yield}}{FOS}\right) \times A$) and the ultimate axial tensile load $P_{tensile}$ (i.e., $\left(\frac{\sigma_{tensile}}{FOS}\right) \times A$) at which the aircraft structure can operate safely were nearly found as $5.7645e + 04 N$ and $7.6148e + 04 N$, respectively. Under these ultimate axial loads, the vibration modes of the channel cross-section aircraft structure were obtained depending on the boundary conditions, and then the results were presented in Figure 20 – Figure 23. As can be seen from these figures, it turns out that the material of the aircraft structure deteriorated much faster under the ultimate axial compressive load than under the ultimate axial tensile load, for the C-F, C-C, and S-S boundary conditions.
- (b) Using the data in reference [39], the cross-sectional area of the aircraft structure with the semi-circle cross-section was found to be $3.08 \times 10^{-4} m^2$. Based on the mechanical properties of aerospace aluminium alloy AL 2024-T351 [34] and FOS for aerospace structures [42], as in the channel cross-section aircraft structure, the ultimate axial compression load P_{yield} and ultimate axial tensile load $P_{tensile}$ were nearly found $6.6528e + 04 N$ and $8.7883e + 04 N$, respectively. Under these ultimate axial crush loads, the vibration modes of the semi-circle cross-section structure were obtained depending on the boundary conditions, and then the results were given in Figures 22 - Figure 24. As can be seen from these figures, it found out that the material of the semi-circle cross-section aircraft structure deteriorates approximately the same amount under the ultimate axial compressive load and under the ultimate axial tensile load in the C-F, C-C, and S-S boundary conditions.
- (c) Based on the data in reference [40], the cross-sectional area of the aircraft structure with the open box cross-section was found to be $8.76e - 04 m^2$. Based on the mechanical properties of aerospace aluminium alloy AL 2024-T351 [34] and FOS for aerospace structures [42], as in the channel cross-section and semi-circle cross-section aircraft structures, the ultimate axial compression load P_{yield} and ultimate axial tensile load $P_{tensile}$ were nearly found $18.9216e + 04 N$ and $24.9952e + 04 N$, respectively. Under these ultimate axial crush loadings, the vibration modes of the open box cross-section aircraft structure were obtained depending on the boundary conditions and then the results were presented in Figures 28 - Figure 30. It was found from these figures that the material of the aircraft structure with the open box cross-section deteriorates much faster under the ultimate axial compressive load than under the ultimate axial tensile load, for the C-F, C-C, and S-S boundary conditions, as in the channel cross-section aircraft structure.

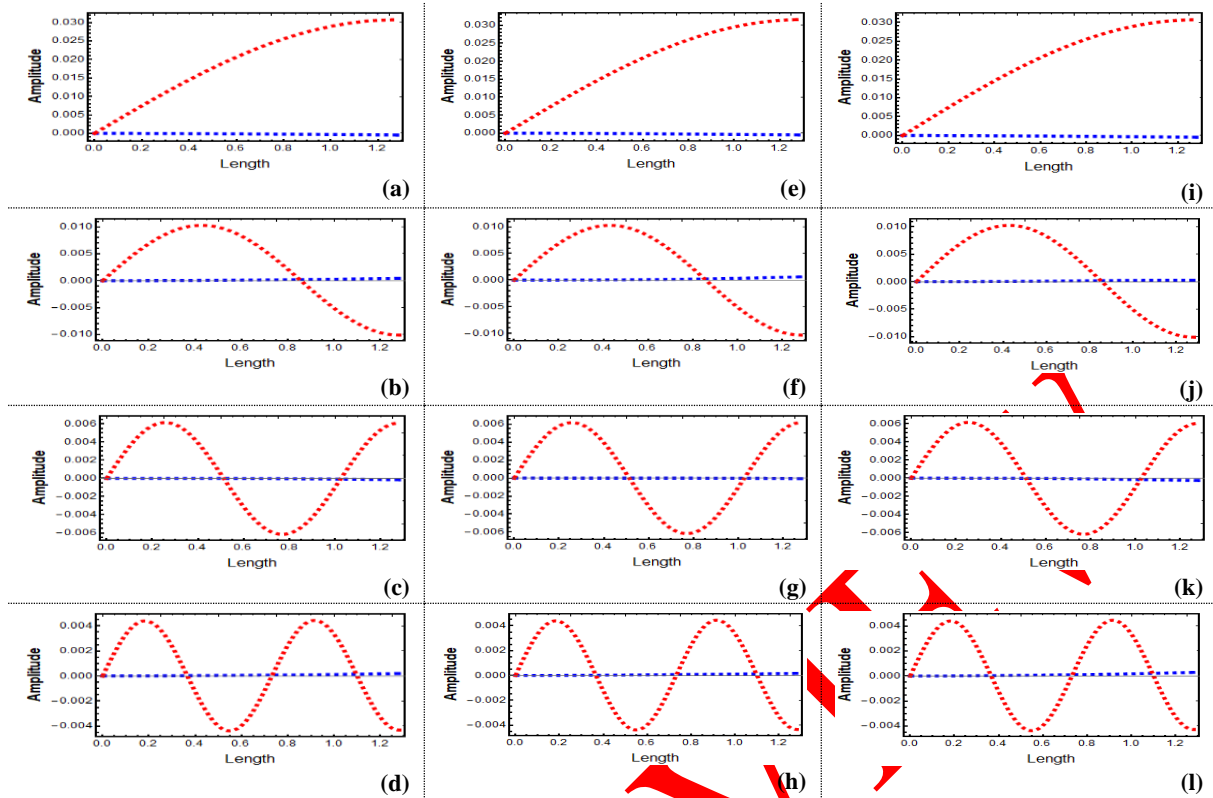


Figure 13. First four consecutive vibration mode shapes of an aircraft structure with channel cross-section for C-F boundary condition (blue: bending, red: torsion), (a)-(d) when $P = 0$ N, (e)-(h) when $P = 2560$ N, and (i)-(l) when $P = -2560$ N

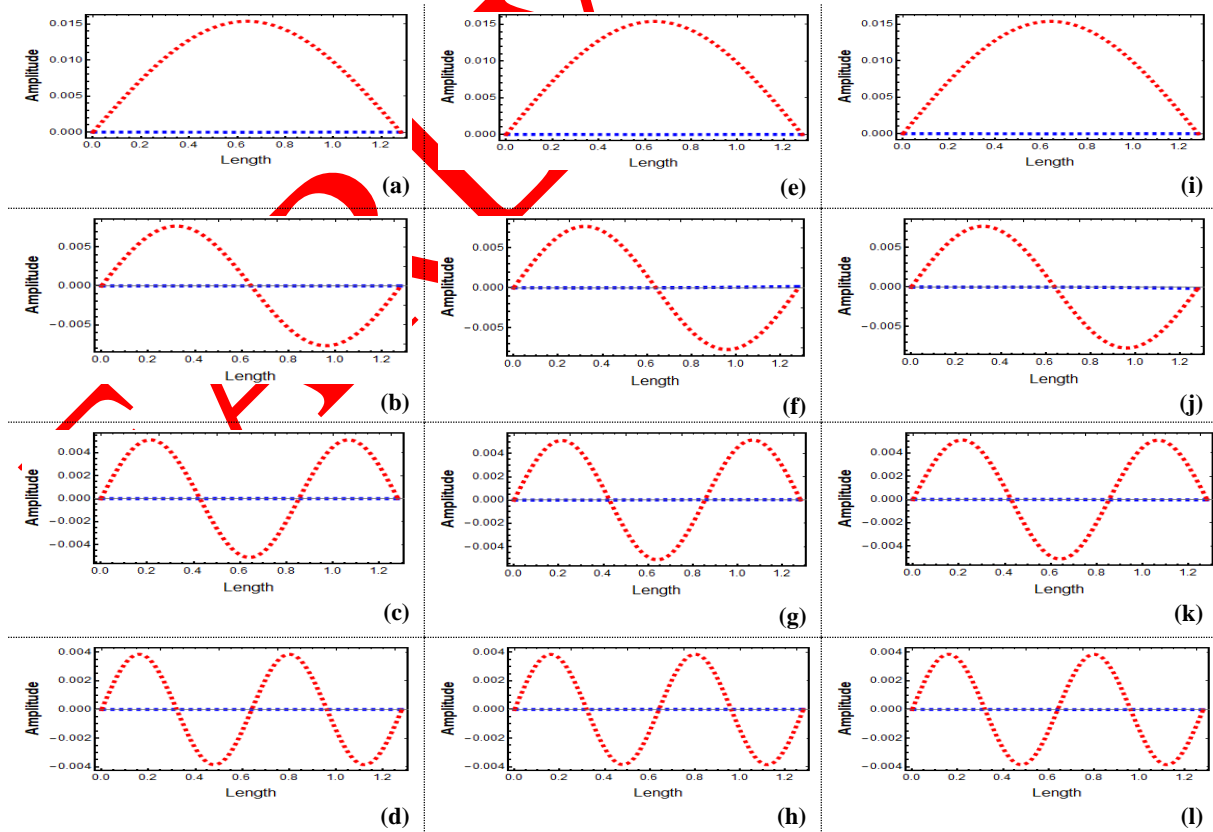


Figure 14. First four consecutive vibration mode shapes of an aircraft structure with channel cross-section for C-C boundary condition (blue: bending, red: torsion), (a)-(d) when $P = 0$ N, (e)-(h) when $P = 2560$ N, and (i)-(l) when $P = -2560$ N

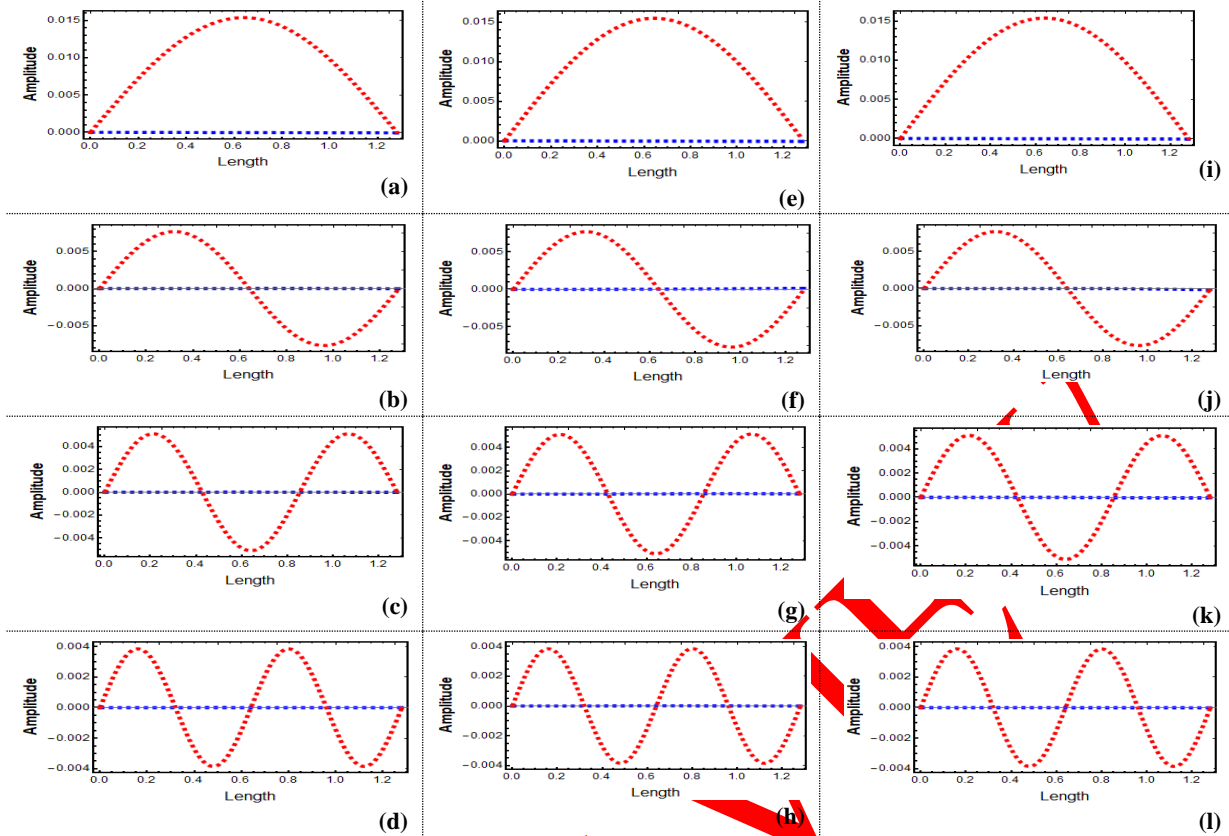


Figure 15. First four consecutive vibration mode shapes of an aircraft structure with channel cross-section for S-S boundary condition (blue: bending, red: torsion), (a)-(d) when $P = 0 \text{ N}$, (e)-(h) when $P = 2560 \text{ N}$, and (i)-(l) when $P = -2560 \text{ N}$

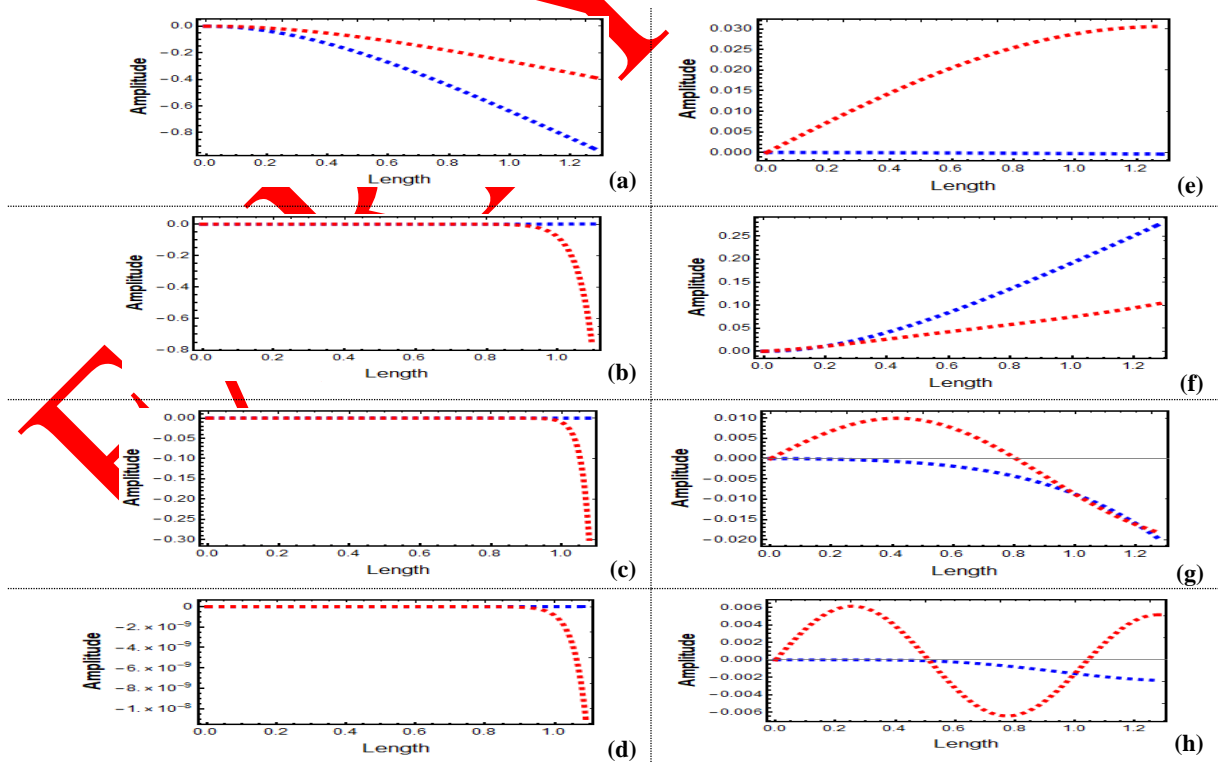


Figure 16. First four consecutive vibration mode shapes of an aircraft structure with channel cross-section for C-F boundary condition (blue: bending, red: torsion), (a)-(d) when $P = 5.7645e + 04 \text{ N}$ (i.e., the ultimate axial compression load), (e)-(h) when $P = -7.6148e + 04 \text{ N}$ (i.e., the ultimate axial tensile load)

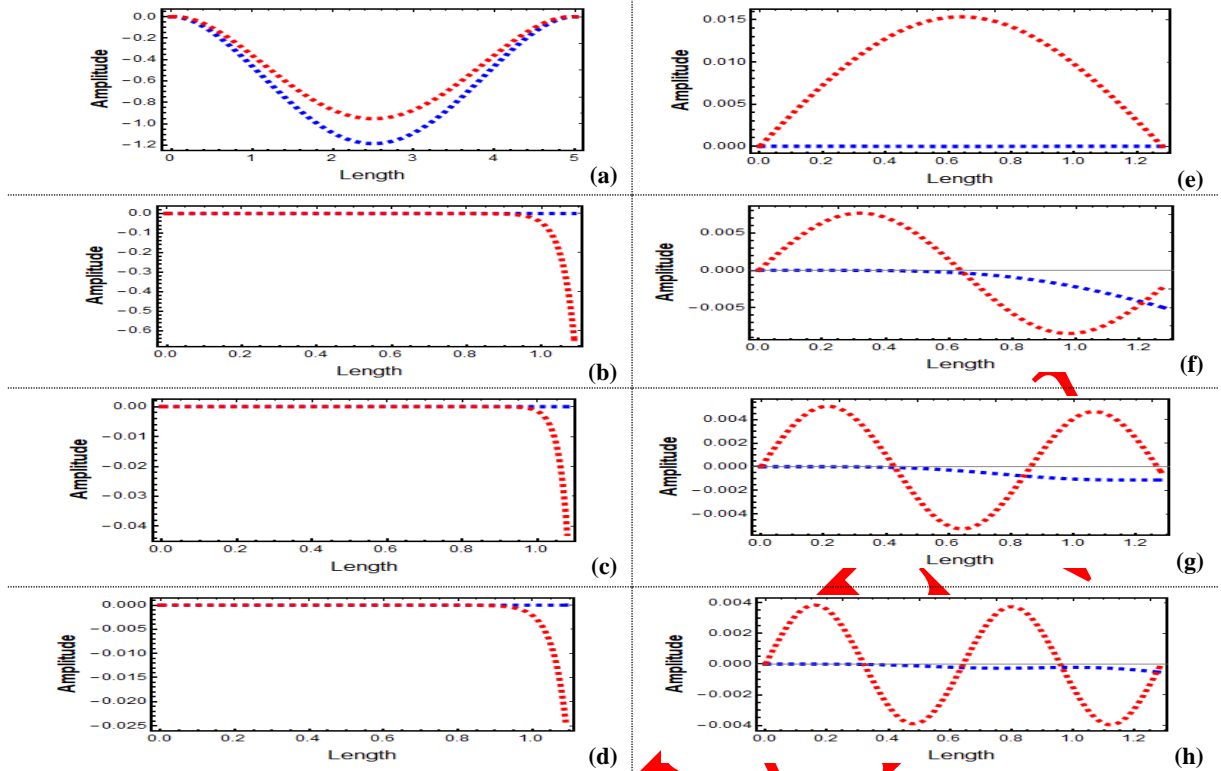


Figure 17. First four consecutive vibration mode shapes of an aircraft structure with channel cross-section for C-C boundary condition (blue: bending, red: torsion), (a)-(d) when $P = 5.7645e + 04 \text{ N}$ (i.e., the ultimate axial compression load), (e)-(h) when $P = -7.6148e + 04 \text{ N}$ (i.e., the ultimate axial tensile load)

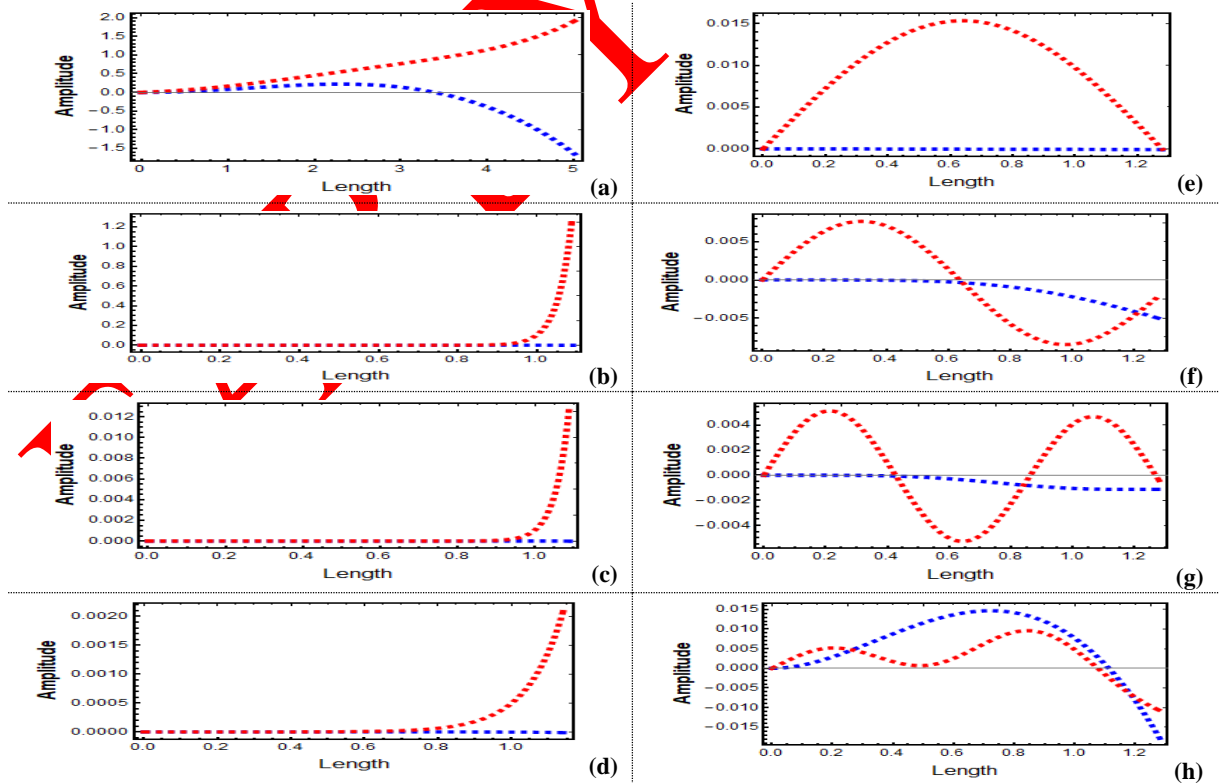


Figure 18. First four consecutive vibration mode shapes of an aircraft structure with channel cross-section for S-S boundary condition (blue: bending, red: torsion), (a)-(d) when $P = 5.7645e + 04 \text{ N}$ (i.e., the ultimate axial compression load), (e)-(h) when $P = -7.6148e + 04 \text{ N}$ (i.e., the ultimate axial tensile load)

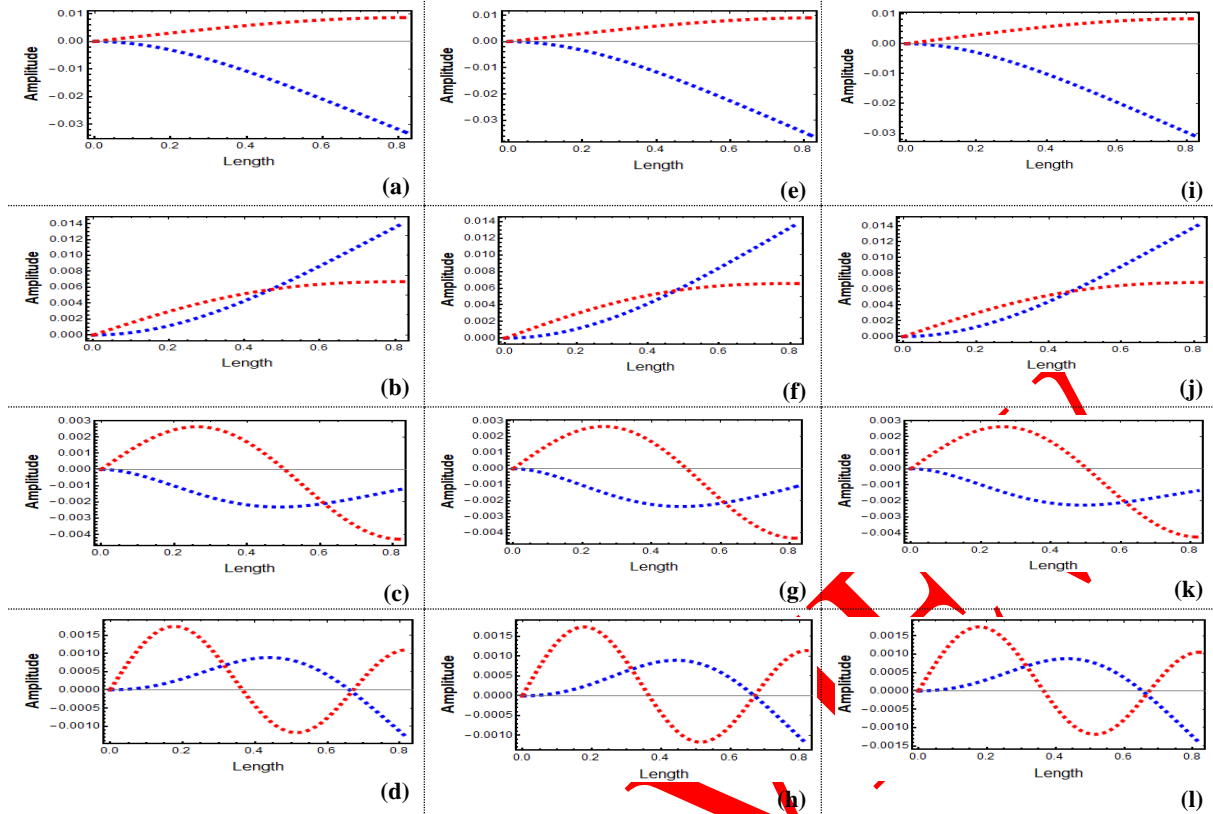


Figure 19. First four consecutive vibration mode shapes of an aircraft structure with semi-circle cross-section for C-F boundary condition (blue: bending, red: torsion), (a)-(d) when $P = 0\text{ N}$, (e)-(h) when $P = 1790\text{ N}$, and (i)-(l) when $P = -1790\text{ N}$

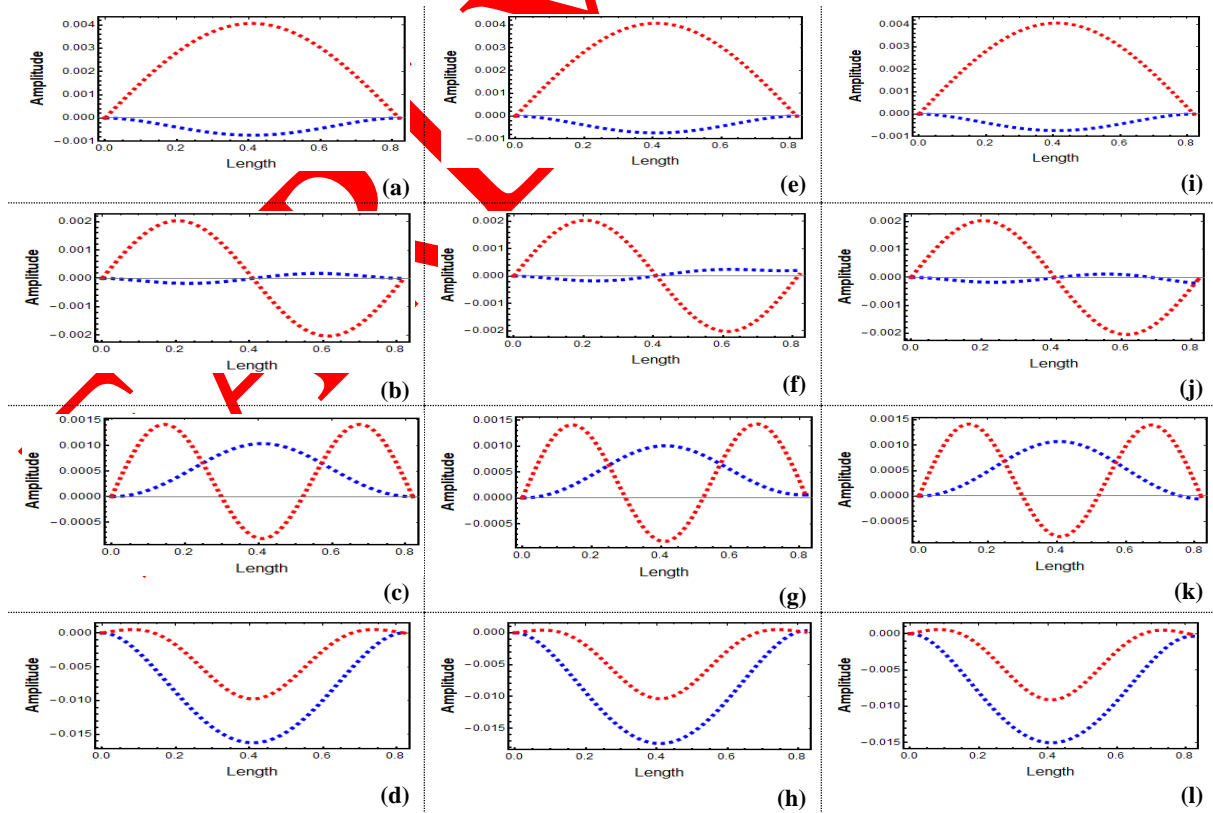


Figure 20. First four consecutive vibration mode shapes of an aircraft structure with semi-circle cross-section for C-C boundary condition (blue: bending, red: torsion), (a)-(d) when $P = 0\text{ N}$, (e)-(h) when $P = 1790\text{ N}$, and (i)-(l) when $P = -1790\text{ N}$

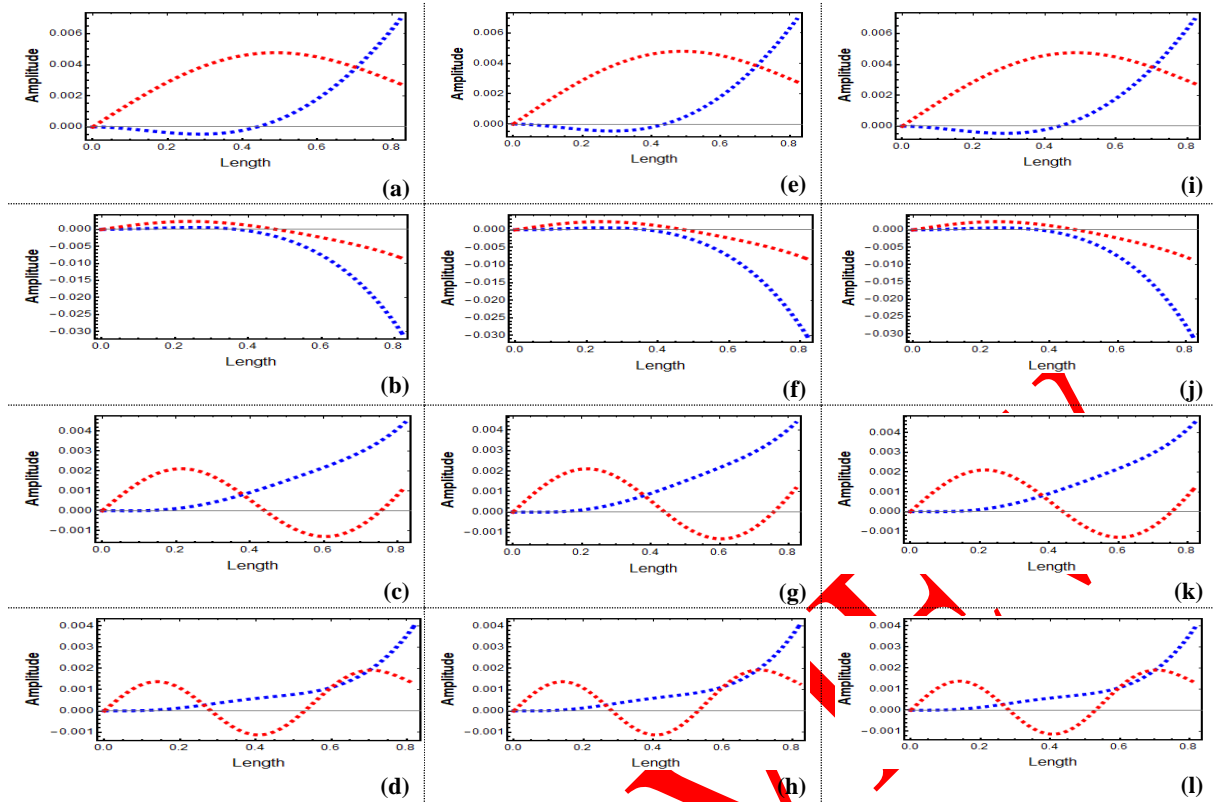


Figure 21. First four consecutive vibration mode shapes of an aircraft structure with semi-circle cross-section for S-S boundary condition (blue: bending, red: torsion), (a)-(d) when $P = 0$ N, (e)-(h) when $P = 1790$ N, and (i)-(l) when $P = -1790$ N

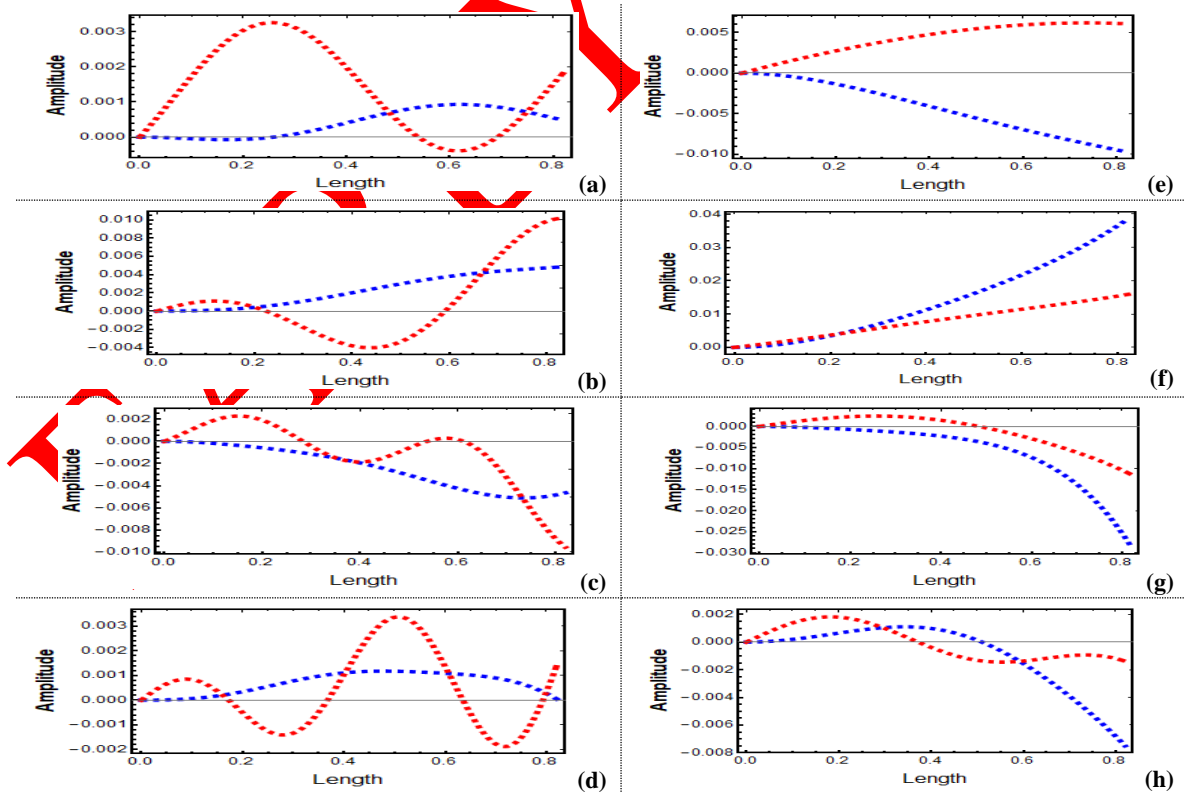


Figure 22. First four consecutive vibration mode shapes of an aircraft structure with semi-circle cross-section for C-F boundary condition (blue: bending, red: torsion), (a)-(d) when $P = 6.6528e + 04$ N (i.e., the ultimate axial compression load), (e)-(h) when $P = -8.7883e + 04$ N (i.e., the ultimate axial tensile load)

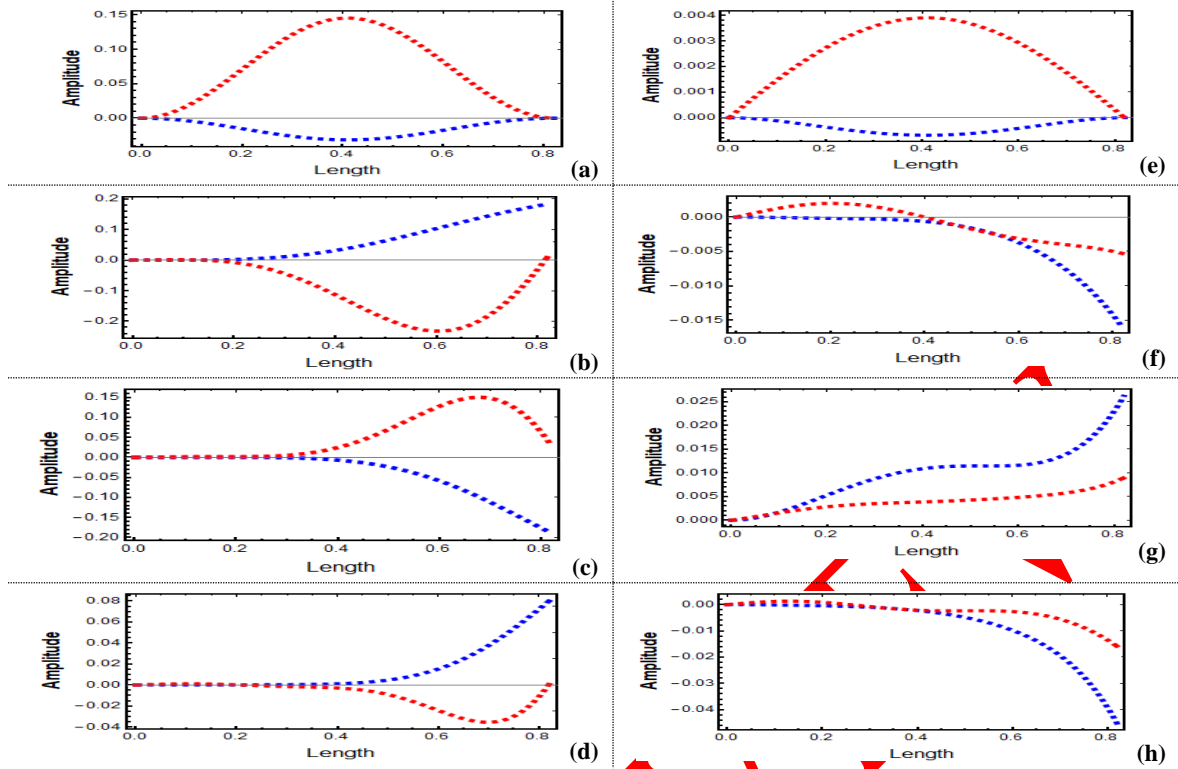


Figure 23. First four consecutive vibration mode shapes of an aircraft structure with semi-circle cross-section for C-C boundary condition (blue: bending, red: torsion), (a)-(d) when $P = 6.6528e + 04 \text{ N}$ (i.e., the ultimate axial compression load), (e)-(h) when $P = -8.7883e + 04 \text{ N}$ (i.e., the ultimate axial tensile load)

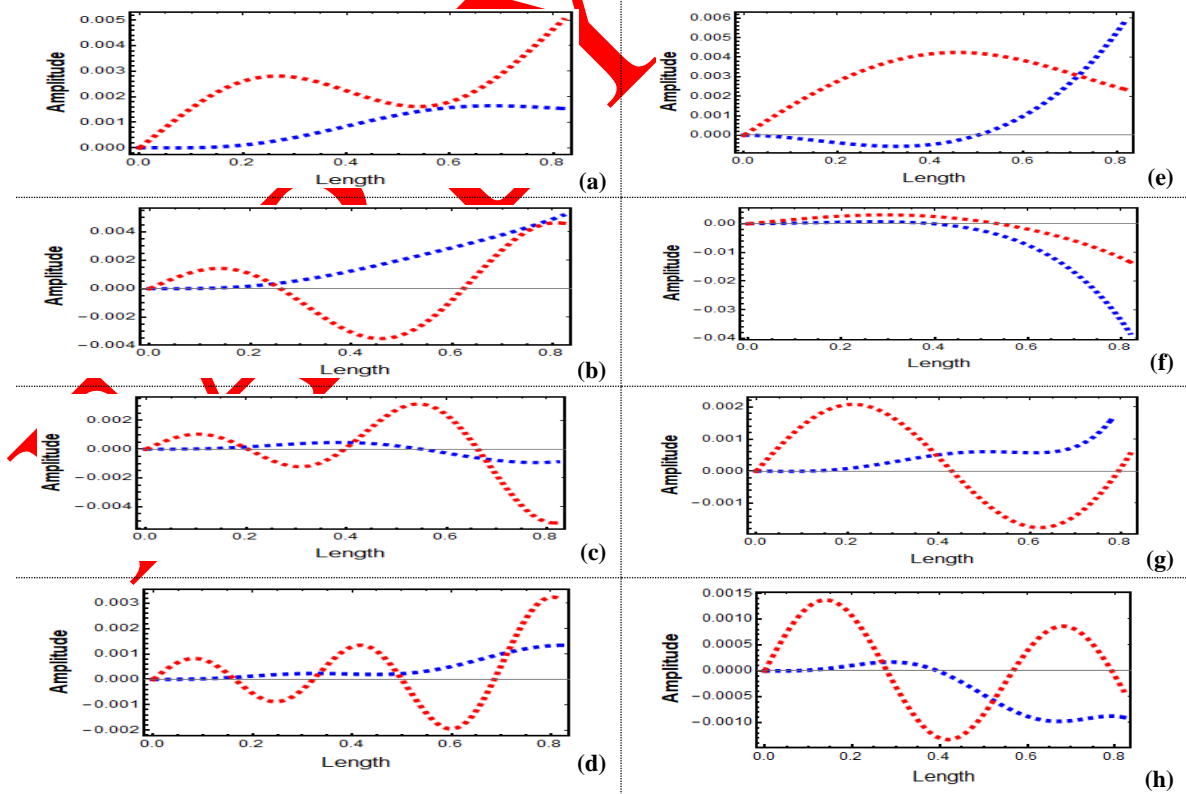


Figure 24. First four consecutive vibration mode shapes of an aircraft structure with semi-circle cross-section for S-S boundary condition (blue: bending, red: torsion), (a)-(d) when $P = 6.6528e + 04 \text{ N}$ (i.e., the ultimate axial compression load), (e)-(h) when $P = -8.7883e + 04 \text{ N}$ (i.e., the ultimate axial tensile load)

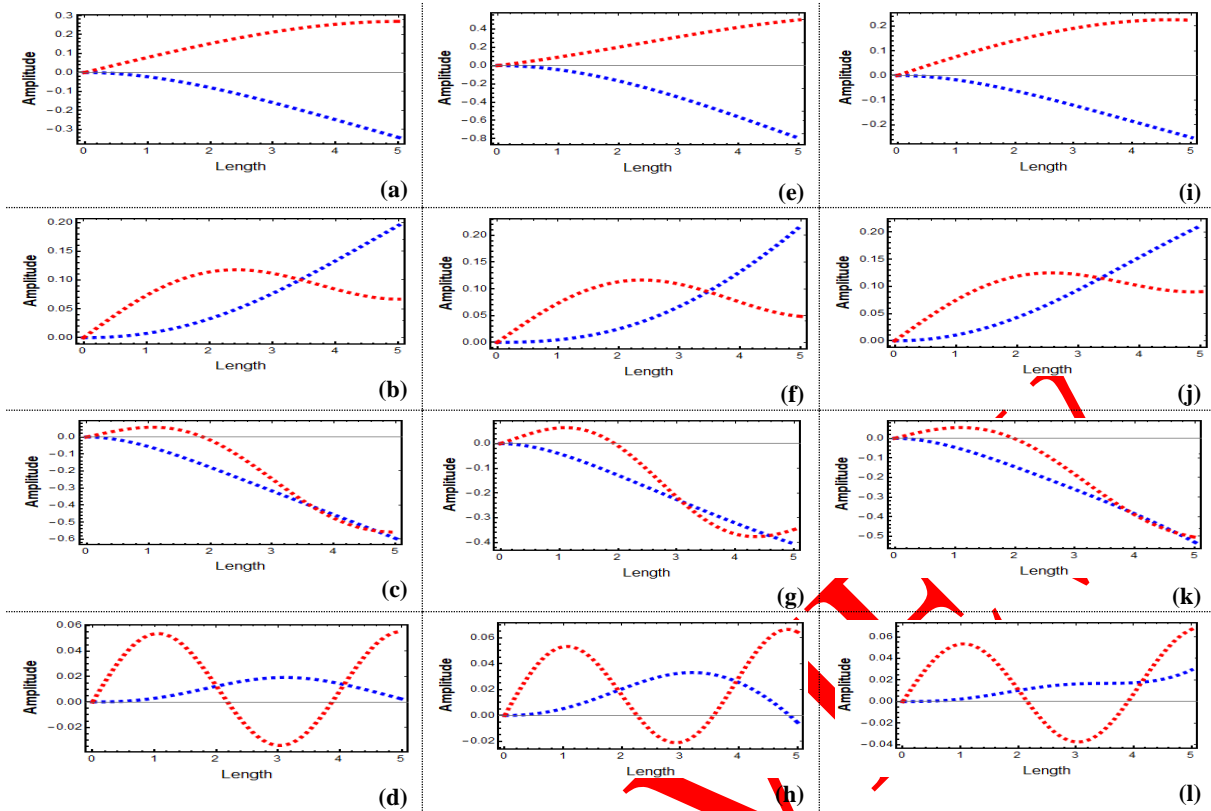


Figure 25. First four consecutive vibration mode shapes of an aircraft structure with open box cross-section for C-F boundary condition (blue: bending, red: torsion), (a)-(d) when $P = 0$ N, (e)-(h) when $P = 2500$ N, and (i)-(l) when $P = -2500$ N

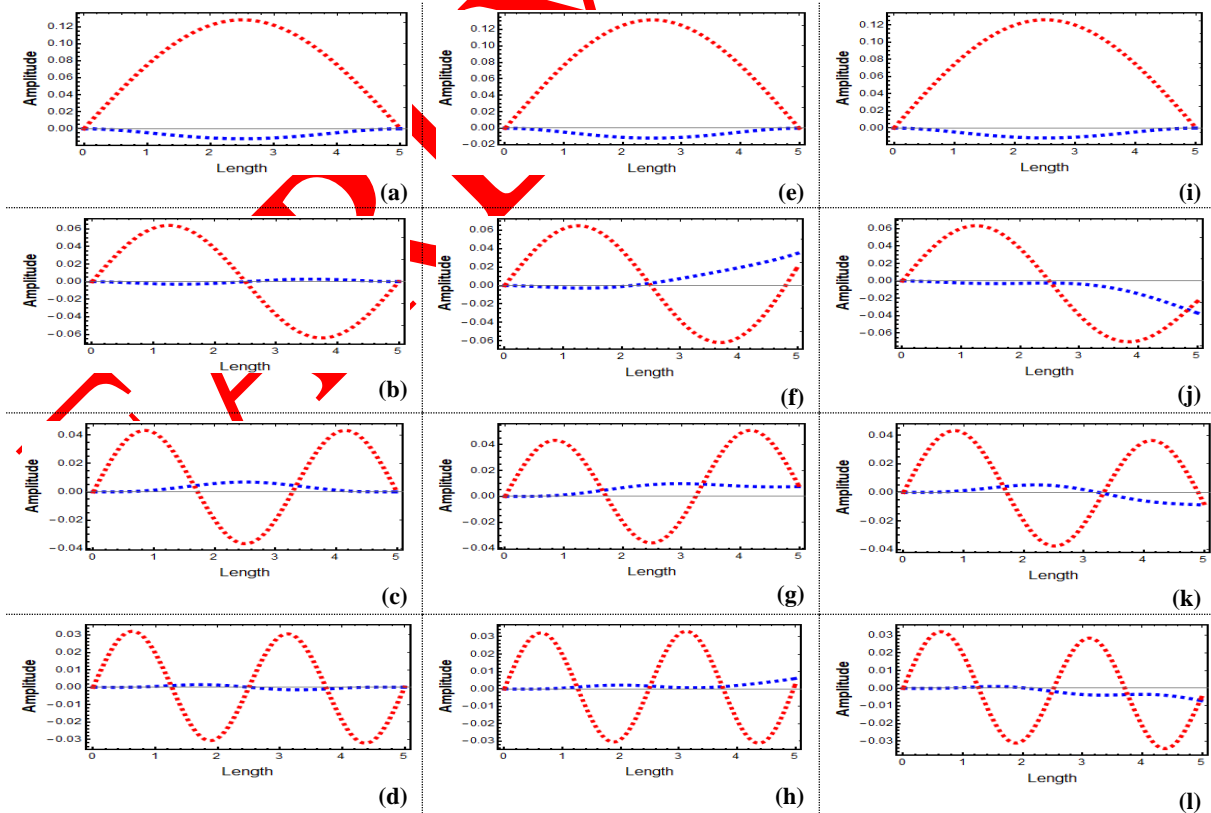


Figure 26. First four consecutive vibration mode shapes of an aircraft structure with open box cross-section for C-C boundary condition (blue: bending, red: torsion), (a)-(d) when $P = 0$ N, (e)-(h) when $P = 2500$ N, and (i)-(l) when $P = -2500$ N

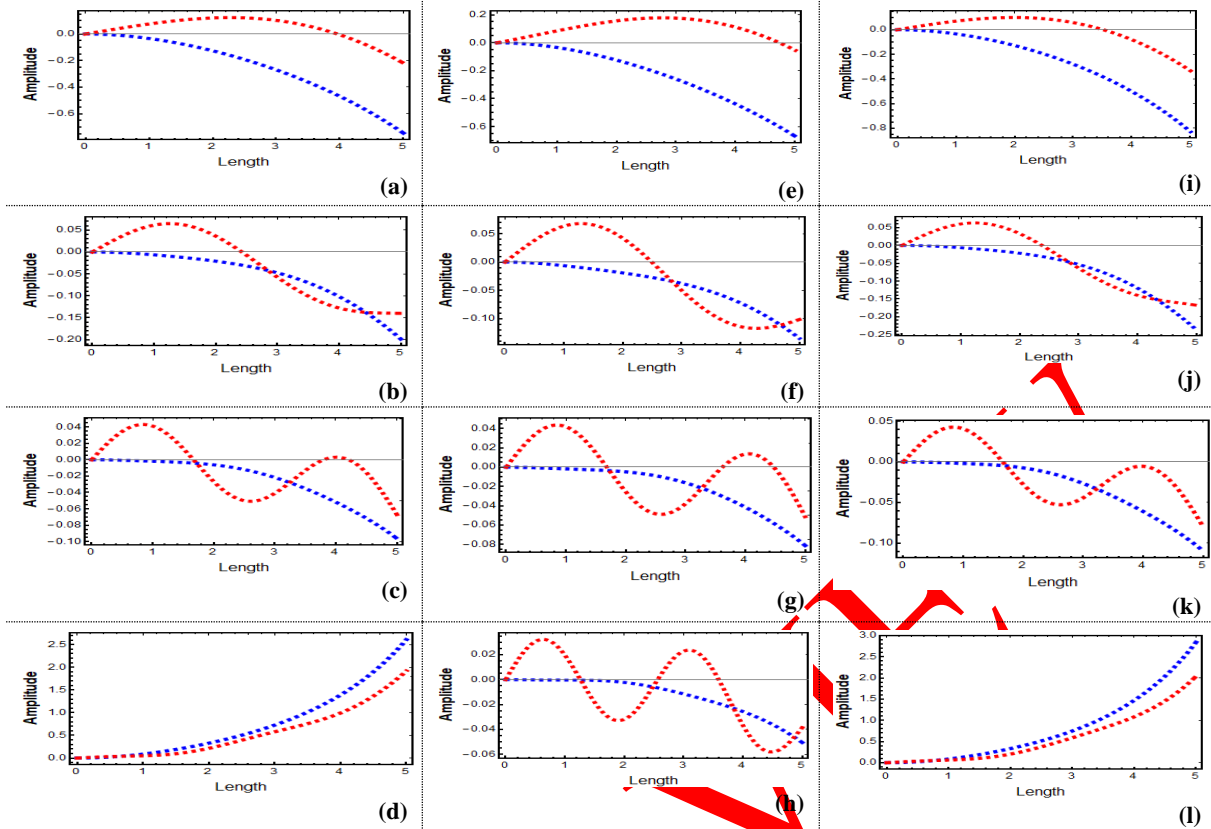


Figure 27. First four consecutive vibration mode shapes of an aircraft structure with open box cross-section for S-S boundary condition (blue: bending, red: torsion), (a)-(d) when $P = 0$ N, (e)-(h) when $P = 2500$ N, and (i)-(l) when $P = -2500$ N

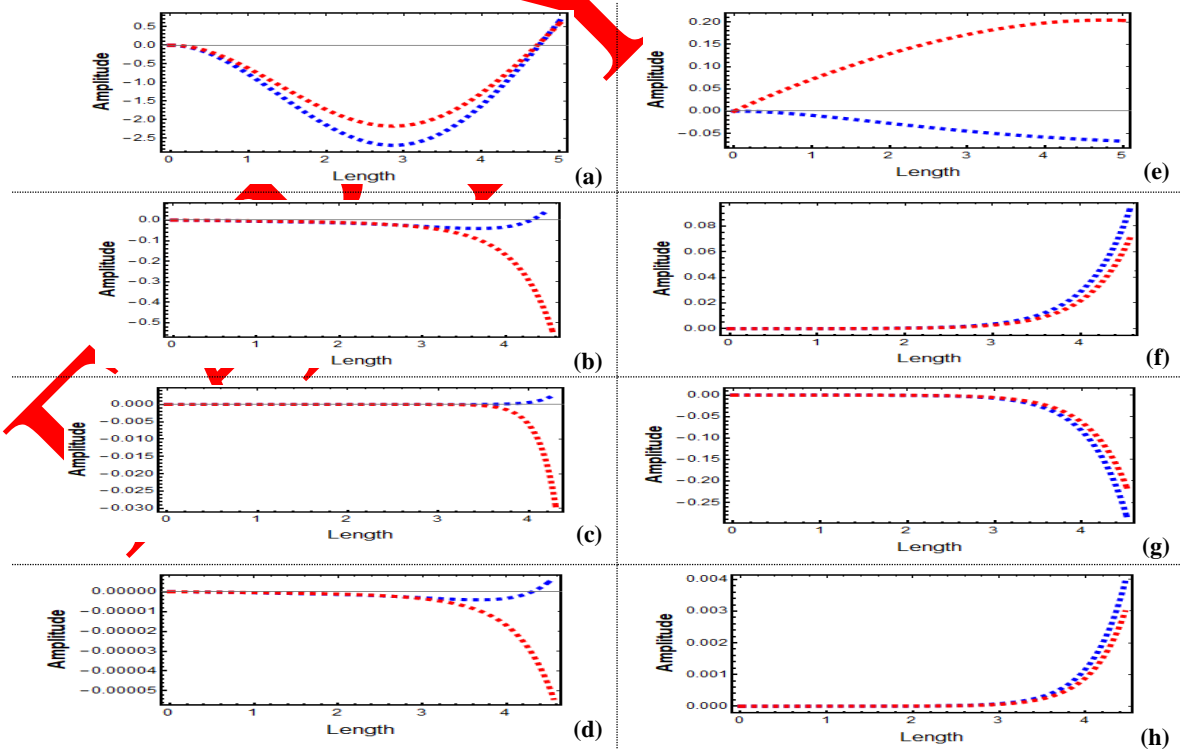


Figure 28. First four consecutive vibration mode shapes of an aircraft structure with open box cross-section for C-F boundary condition (blue: bending, red: torsion), (a)-(d) when $P = 18.9216e + 04$ N (i.e., the ultimate axial compression load), (e)-(h) when $P = -24.9952e + 04$ N (i.e., the ultimate axial tensile load)

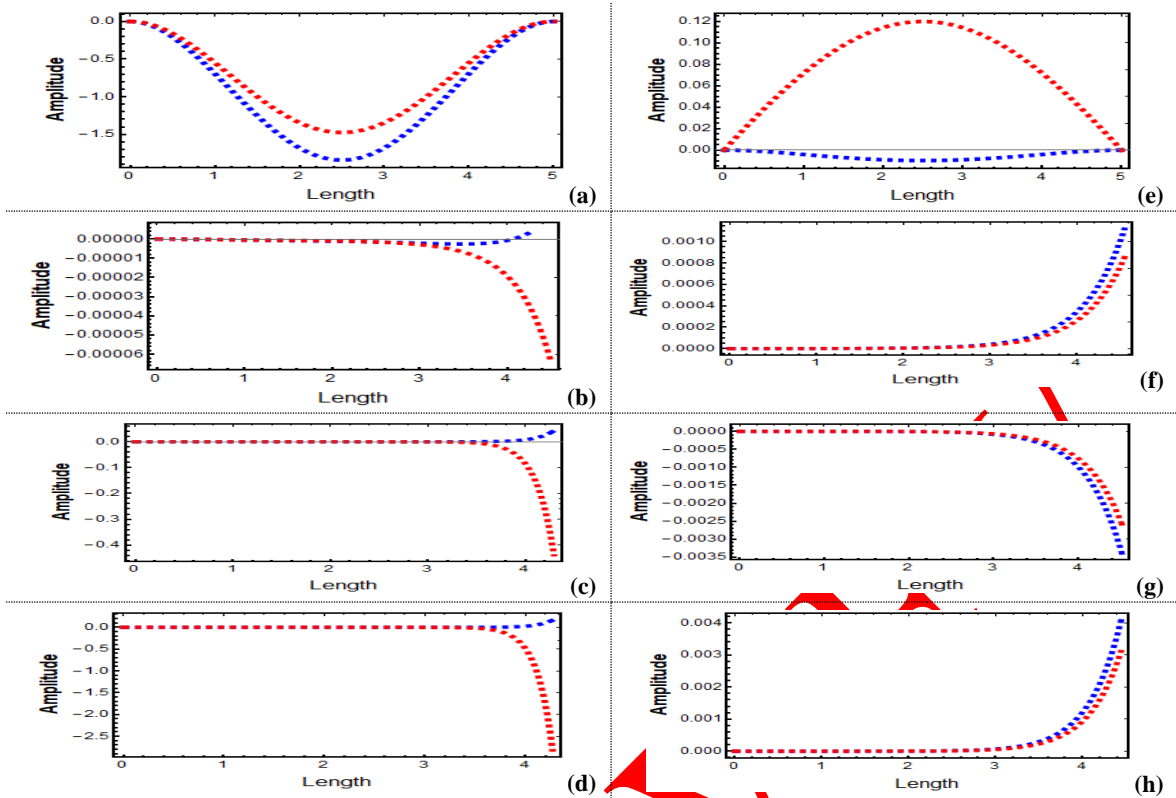


Figure 29. First four consecutive vibration mode shapes of an aircraft structure with open box cross-section for C-C boundary condition (blue: bending, red: torsion), (a)-(d) when $P = 18.9216e + 04 \text{ N}$ (i.e., the ultimate axial compression load), (e)-(h) when $P = -24.9952e + 04 \text{ N}$ (i.e., the ultimate axial tensile load)

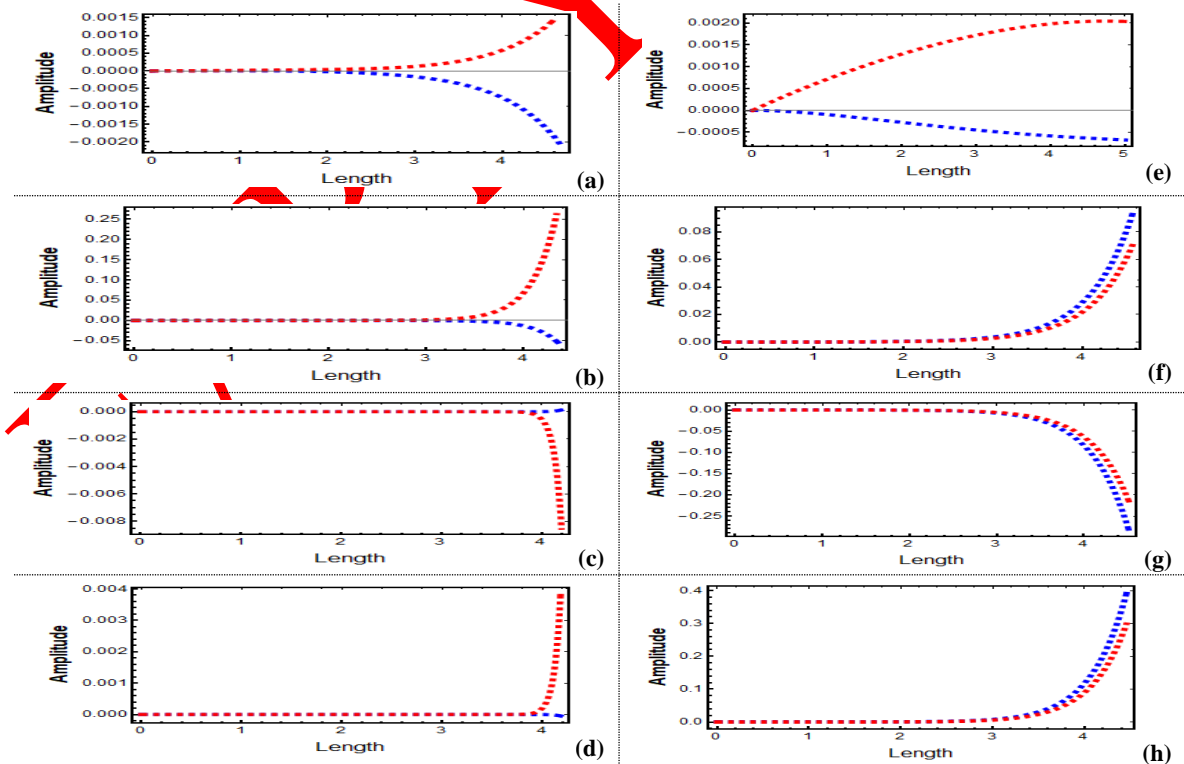


Figure 30. First four consecutive vibration mode shapes of an aircraft structure with open box cross-section for S-S boundary condition (blue: bending, red: torsion), (a)-(d) when $P = 18.9216e + 04 \text{ N}$ (i.e., the ultimate axial compression load), (e)-(h) when $P = -24.9952e + 04 \text{ N}$ (i.e., the ultimate axial tensile load)

4. CONCLUSION

Terminologically, crashworthiness refers to the capacity of a structural system subjected to a crush loading to dissipate kinetic impact energy on its own through a controlled and predictable deformation. In the aviation industry, structural components of an aircraft exposed to a crush loading play a leading role in the distribution of the kinetic energy and absorption of impact energy. In this study, vibration analysis of an aircraft structure exposed to an axial crush loading was dealt with in terms of crashworthiness of the aircraft structure. For this purpose, firstly, a mathematical model of an aircraft structure subjected to an axial crush loading was derived by using the extended Hamilton principle. Subsequently, the mathematical model derived was solved by using differential transform method for various boundary conditions of the aircraft structure. Then, three different applications were carried out to determine the vibration response of the aircraft structure to the axial crush loading for various boundary conditions and cross-section of the aircraft structure.

Depending on the findings that were obtained in this study, the results of the study were found that:

- In order to attain the first six convergent vibration frequencies of an aircraft structure, the number of terms included in DTM varies depending on the cross-section and boundary condition of the aircraft structure.
- Regardless of the direction of the axial crush loading, the geometric coupling term has a reduce effect for the C-F boundary condition and almost no effect for the C-C and S-S boundary conditions for the channel cross-section aircraft structure; on the other hand, there is no any specific effect (for instance, increase or reduce effect) of the geometric coupling term on the vibration frequencies of the semi-circle and open box cross-section aircraft structures irrespective of the type of the boundary condition and direction of the axial crush loading.
- The vibration mode shapes of an aircraft structure are affected by the boundary conditions of the aircraft structure, cross-section of the aircraft structure, magnitude of the axial load applied to the aircraft structure, and direction of the axial load applied.
- Relative measurements of the displacement between bending motion and torsional motion for the C-F, C-C and S-S boundary conditions showed that in the vibration modes generated for the channel cross-section aircraft structure, the torsional motion is particularly evident in the first five modes while in the vibration modes generated for the semi-circle and open box cross-section aircraft structures, all vibration modes are in coupled mode in the first five modes.
- For the C-F, C-C, and S-S boundary conditions, the material of an aircraft structure with the channel cross-section and open box cross-section deteriorates much faster under the ultimate axial compressive load than under the ultimate axial tensile load; however, the material of an aircraft structure with the semi-circle cross-section deteriorates approximately the same amount under the ultimate axial compressive load and under the ultimate axial tensile load.

Based on these results, it can be concluded that the geometry of the aircraft structure, boundary condition of the aircraft structure, material of the aircraft structure, magnitude of an axial crush loading applied to the aircraft structure, and direction of the axial load plays significant role in the change of vibration characteristics of an aircraft structure. Moreover, as can be noticed from this study, the contribution of the design of considered thin-walled beam to the crash resistance of an aircraft structure varies depending on which component the thin-walled beam represents in the aircraft. Depending on the boundary condition and the geometry, it can sometimes be a complete aircraft wing or fuselage, while it can sometimes be a spar, strut, or support on an aircraft wing. For this reason, the thin-walled beam that represents an aircraft structure in this study was not customized as a specific aircraft structure but evaluated the vibration analysis of the thin-walled beam with respect to various parameters making up the structure in terms of the crashworthiness of the structure. Thus, we left the customization of the aircraft structure (i.e., the thin-walled beam considered in the study) within the scope that can be integrated according to the problem of researchers doing research on this subject.

CONFLICTS OF INTEREST

No conflict of interest was declared by the authors.

REFERENCES

- [1] Grote, M., Williams, I., Preston, J., “Direct carbon dioxide emissions from civil aircraft,” *Atmospheric Environment*, 95: 214–224, (2014). DOI: 10.1016/j.atmosenv.2014.06.042.
- [2] Prabandari, A.P., Puteri, E.A.P., “Standardization of Private Aircraft: Implications of Climate Change,” in *IOP Conference Series: Earth and Environmental Science*, IOP Publishing, 012028, (2023). DOI: 10.1088/1755-1315/1270/1/012028.
- [3] Anand, S., Alderliesten, R., Castro, S.G., “Low-fidelity crashworthiness assessment of unconventional aircraft: Modeling of plastic bending,” *AIAA SCITECH 2024*, 0833, (2024).
- [4] Kurtaran, H., Eskandarian, A., Marzougui, D., Bedewi, N.E., “Crashworthiness design optimization using successive response surface approximations,” *Computational mechanics*, 29(4–5): 409–421, (2002). DOI: 10.1007/s00466-002-0351-x.
- [5] Wang, T., Wang, L., Wang, C., Zou, X., “Crashworthiness analysis and multi-objective optimization of a commercial vehicle frame: A mixed meta-modeling-based method,” *Advances in Mechanical Engineering*, 10(5), (2018). DOI: 10.1177/1687814018778480.
- [6] Guida, M., Marulo, F., Abrate, S., “Advances in crash dynamics for aircraft safety,” *Progress in Aerospace Sciences*, 98: 106–123, (2018). DOI: 10.1016/j.paerosci.2018.03.008.
- [7] Xue, P., Ding, M.L., Qiao, C.F., Yu, T.X., “Crashworthiness Study of a Civil Aircraft Fuselage Section,” *Latin American Journal of Solids and Structures*, 11: 1615–1627, (2014).
- [8] Guida, M., Lamanna, G., Marulo, F., Caputo, F., “Review on the design of an aircraft crashworthy passenger seat,” *Progress in Aerospace Sciences*, 129, (2022).
- [9] Garofano, A., Sellitto, A., Acanfora, V., Di Caprio, F., Riccio, A., “On the effectiveness of double-double design on crashworthiness of fuselage barrel,” *Aerospace Science and Technology*, 140, (2023). DOI: 10.1016/j.ast.2023.108479.
- [10] Mou, H., Chen, Y., Feng, Z., Liu, H., “Damage and energy absorption behavior of CFRP/aluminum hybrid open-section thin-walled columns subjected to quasi-static loading,” *Thin-Walled Structures*, 197, (2024). DOI: 10.1016/j.tws.2024.111593.
- [11] Li, Q., Xiao, Q., Liu, X., Cheng, X., Mao, C., Hu, H., “Hierarchical double-hat beam for axial crashworthiness,” *Aerospace Science and Technology*, 141, (2023). DOI: 10.1016/j.ast.2023.108515.
- [12] Tang, T., Zhang, W., Yin, H., Wang, H., “Crushing analysis of thin-walled beams with various section geometries under lateral impact,” *Thin-Walled Structures*, 102: 43–57, (2016). DOI: 10.1016/j.tws.2016.01.017.
- [13] Fanthorpe, C., Soban, D., Price, M., Butterfield, J., “Developing a capability function relating aircraft systems cost overruns to aircraft design parameters,” in *11th AIAA Aviation Technology, Integration, and Operations (ATIO) Conference, including the AIAA Balloon Systems Conference and 19th AIAA Lighter-Than-Air Technology Conference*, (2011). DOI: 10.2514/6.2011-6837.
- [14] Lobitz, L., Hahn, A., Vogt, D., Luplow, T., Michalowski, P., Heimbs, S., Garnweitner, G., “Conceptual Challenges for Crashworthy Battery-Electric Commercial Aircraft – A Review,” in *AIAA SCITECH 2024 Forum*, Reston, Virginia: American Institute of Aeronautics and Astronautics, (2024). DOI: 10.2514/6.2024-2156.

- [15] Liang, H., Liu, B., Pu, Y., Sun, H., Wang, D., "Crashworthiness analysis of variable thickness CFRP/Al hybrid multi-cell tube," *International Journal of Mechanical Sciences*, 266, (2024). DOI: 10.1016/j.ijmecsci.2024.108959.
- [16] Xue, P., Wang, L., Qiao, C.F., "Crashworthiness Study on Fuselage Section and Struts under Cabin Floor," *International Journal of Protective Structures*, 4(2): 515-525, (2011). DOI: 10.1260/2041-4196.2.4.515
- [17] Ren, Y., Xiang, J., "A comparative study of the crashworthiness of civil aircraft with different strut configurations," *International Journal of Crashworthiness*, 15(3): 321-330, (2010). DOI: 10.1080/13588260903343823.
- [18] Ren, Y., Xiang, J., "Influences of Geometrical factors on the crashworthiness of open shells," in *In 51st AIAA/ASME/ASCE/AHS/ASC Structures, Structural Dynamics, and Materials Conference*, 1-10, (2010).
- [19] Ren, Y., Xiang, J., "Energy absorption structures design of civil aircraft to improve crashworthiness," *Aeronautical Journal*, 118(1202): 383-398, (2014). DOI: 10.1017/S0001924000009180.
- [20] Patil, S., Pangavhane, D., "Crashworthiness analysis and multiobjective optimization for variable thickness square thin-wall columns under axial loading," *Materials Today: Proceedings*, 77: 860-870, (2023). DOI: 10.1016/j.matpr.2022.11.506
- [21] Moas, E., Boitnott, R.L., Griffin, H., "An Analytical and Experimental Investigation of the Response of the Curved, Composite Frame/Skin Specimens," *Journal of the American Helicopter Society*, 39(3): 58-66, (1994).
- [22] Woodson, M.B., Johnson, E.R., Haftka, R.T., "Optimal design of composite fuselage frames for crashworthiness," *International Journal of Crashworthiness*, 1(4): 369-380, (1996). DOI: 10.1533/cras.1996.0027.
- [23] Collins, J.S., Johnson, E.R., "Static and Dynamic Response of Graphite-Epoxy Curved Frames," *Journal of Composite Materials*, 26(6): 792-803, (1992). DOI: <https://doi.org/10.1177/002199839202600602>.
- [24] Perez, J.G., Johnson, E.R., Boitnott, R.L., "Design and test of semicircular composite frames optimized for crashworthiness," in *Collection of Technical Papers-AIAA/ASME/ASCE/AHS/ASC Structures, Structural Dynamics and Materials Conference*, AIAA, 27-38, (1998). DOI: 10.2514/6.1998-1703.
- [25] Zhang, C., Bimenda, W.K., Horvat, F.E., Wang, W., "Application of numerical methods for crashworthiness investigation of a large aircraft wing impact with a tree," *Mathematical & Computational Forestry & Natural Resource Science*, 5(1), 71-85, (2013).
- [26] Xie, C., Wang, D., Zong, L., Kong, D., "Crashworthiness analysis and multi-objective optimization of spatial lattice structure under dynamic compression," *International Journal of Impact Engineering*, 180(104713), 1-15, (2023).
- [27] Bildik, N., Konuralp, A., Bek, F.O., Küçükarslan, S., "Solution of different type of the partial differential equation by differential transform method and Adomian's decomposition method," *Applied Mathematics and Computation*, 172(1): 551-567, (2006).

- [28] Odibat, Z.M., Bertelle, C., Aziz-Alaoui, M.A., Duchamp, G.H.E., "A multi-step differential transform method and application to non-chaotic or chaotic systems," *Computers and Mathematics with Applications*, 59(4): 1462–1472, (2010). DOI: 10.1016/j.camwa.2009.11.005.
- [29] Yaghoobi, H., Torabi, M., "The application of differential transformation method to nonlinear equations arising in heat transfer," *International Communications in Heat and Mass Transfer*, 38(6): 815–820, (2011). DOI: 10.1016/j.icheatmasstransfer.2011.03.025.
- [30] Shen, R., Hua, H., Jin, X., "Bending-torsional coupled dynamic response of axially loaded composite Timosenko thin-walled beam with closed cross-section," *Composite Structures*, 64(1): 23–35, (2004). DOI: 10.1016/S0263-8223(03)00210-1.
- [31] Chemartin, L., Lalande, P., Chazottes, A., Elias, P.Q. Delalandre, B.G., Lago, F., "Direct Effects of Lightning on Aircraft Structure: Analysis of the Thermal, Electrical and Mechanical Constraints," *Aerospace Lab*, 5: 1–15, (2012), [Online]. Available: <https://hal.science/hal-01184416>.
- [32] Soysal, A., Ozkol, I., Uzal, E., "An Analytical-Based Lightning-Induced Damage Model for an Aircraft Wing Exposed to Pressure Loading of Lightning," *Mathematical Problems in Engineering*, 2024: 1–17, (2024). DOI: 10.1155/2024/8313135.
- [33] Hashemi, S.M., Richard, M.J., "Free vibrational analysis of axially loaded bending-torsion coupled beams: a dynamic finite element," *Computers & Structures*, 77: 711–724, (2000). [Online]. Available: www.elsevier.com/locate/compstruc.
- [34] Dursun, T., Soutis, C., "Recent developments in advanced aircraft aluminium alloys," *Materials & Design*, 56: 862–871, (2014). DOI: 10.1016/j.matdes.2013.12.002.
- [35] Zhou, J.K., "Differential transformation and its applications for electrical circuits", Wuhan: Huazhong University Press, (1986).
- [36] Soysal, A., Özkol, İ., Uzal, E., "Flexural-torsional-coupled vibration analysis of Euler-Bernoulli beam by using the differential transform method," *Academic Perspective Procedia*, 5(3): 26–33, (2022). DOI: 10.33793/acperpro.05.03.642.
- [37] Banerjee, J.R., Guot, S., Howson, W.P., "Exact Dynamic Stiffness Matrix of a Bending-Torsion Coupled Beam Including Warping," *Computers & Structures*, 59(4):613–621, (1996).
- [38] Jun, L., Rongying, S., Hongxing, H., Xianding, J., "Coupled bending and torsional vibration of axially loaded Bernoulli-Euler beams including warping effects," *Applied Acoustics*, 65(2): 153–170, (2004). DOI: 10.1016/j.apacoust.2003.07.006.
- [39] Banerjee, J.R., Fisher, S.A., "Coupled bending–torsional dynamic stiffness matrix for axially loaded beam elements," *International Journal for Numerical Methods in Engineering*, 33(4): 739–751, (1992). DOI: 10.1002/nme.1620330405.
- [40] Banerjee, J.R., "Coupled bending-torsional dynamic stiffness matrix for beam elements," *International Journal for Numerical Methods in Engineering*, 28: 1283–1298, (1989).
- [41] Eslimy-Isfahany, S.H.R., Banerjee, J.R., "Use of generalized mass in the interpretation of dynamic response of bending-torsion coupled beams," *Journal of Sound and Vibration*, 238(2): 295–308, (2000). DOI: 10.1006/jsvi.2000.3160.

- [42] Larsen, C.E., Raju, I.S., “Moving aerospace structural design practice to a load and resistance factor approach,” in 57th AIAA/ASCE/AHS/ASC Structures, Structural, Dynamics, and Material Conference, 230, (2016).

EARLY VIEW